이학박사 학위논문

급성골수성백혈병에서 KIT과 MYH8 유전자 변이에 대한 기능 분석

Functional study of KIT and MYH8 mutations in acute myeloid leukemia

2019년 8월

서울대학교 대학원

의과대학 협동과정 종양생물학 전공

박 혜 주

ABSTRACT

Functional study of KIT and MYH8 mutations in acute myeloid leukemia

Hyejoo Park

Major in Cancer Biology

Interdisciplinary Graduate Program

The Graduate School

Seoul National University

Acute myeloid leukemia (AML) is a hematologic malignancy in which immature myeloid cells such as myeloblast proliferate abnormally in the bone marrow and normal haematopoiesis is inhibited. Despite initial gratifying response to chemotherapy, almost half of the patients will experience relapse with ultimate failure to achieve long-term remission.

The next-generation sequencing revealed that mutations of *FLT3*, *NPM1*, *DMNT3A*, and *IDH1/2* were the major

pathogenic mutations in acute myeloid leukemia, but the cure rate is still unsatisfactory due to the high heterogeneity of cancer cells, causing relapse. Therefore, in order to improve the cure rate, deeper understanding of mutations and new target discovery are urgently needed.

In the first part, our data showed that upregulated Pim kinase was a novel molecular event in *KIT* D816V which is found frequently in core binding factor (CBF)-AMLs and is associated with a poor prognosis. Through molecular screening, highly upregulated Pim kinases were found in D816V cells and these were involved in proliferation, survival, migration, and drug resistance in the D816V mutant cells. Furthermore, our data demonstrate that upregulated Pim kinases was a unique feature of *KIT* D816V cells, compared with N822K (another c-Kit activating mutation) and N822 made by CRISPR-Cas9 genome editing. Taken together, these results suggest that increased Pim kinases play an important role in the biologic behavior of *KIT* D816V cells and could be a novel therapeutic target in patients with *KIT* D816V mutation.

In the second part, our data showed changes in cellular behavior conferred by *MYH8* R1292X. Novel truncating mutation, *MYH8* R1292X, was discovered by whole-exome sequencing and targeted

resequencing in 209 AML samples. Until now, the role of *MYH8* mutation has not been studied in AML. To investigate the molecular changes in *MYH8* R1292X on cells, we established knock-in cell lines using CRISPR-Cas9 genome editing. The *MYH8* R1292X mutant cells had enhanced migration ability that was confirmed by immunofluorescence staining, wound healing, and adhesion assay. The cell morphology and cell cycle were altered to facilitate migration. Further, epithelial to mesenchymal transition (EMT) transcription factors were increased in the mutant cells and we found that the Raf/MAPK pathway was a major regulator of these characteristics. Collectively, our data suggested that the novel *MYH8* truncating mutation, R1292X is associated with AML progression.

Keywords: Acute myeloid leukemia, *KIT*, Pim kinase, *MYH8*, Truncation mutation, cell migration, cell survival, epithelial-mesenchymal transition

Student Number: 2014-22027

TABLE OF CONTENTS

Ⅱ. A NOVEL TRUNCATION MUTATION, MYH8 R1292X IN AML, INDUCES MORPHOLOGICAL CHANGE, CELL MIGRATION, AND EPITHELIAL TO MESENCHYMAL TRANSITION VIA RAF/MAPK PATHWAY

LIST OF TABLES AND FIGURES

Ⅰ. ROLE OF UPREGULATED PIM KINASES IN COORDINATING SURVIVAL, MIGRATION, AND DRUG RESPONSE IN KIT D816V-MUTATED LEUKEMIC CELLS

Ⅱ. A NOVEL TRUNCATION MUTATION, MYH8 R1292X IN AML, INDUCES MORPHOLOGICAL CHANGE, CELL MIGRATION, AND EPITHELIAL TO MESENCHYMAL TRANSITION VIA RAF/MAPK PATHWAY

Ⅰ. Role of upregulated Pim kinases in coordinating survival, migration, and drug response in *KIT* D816V-mutated leukemic cells

ABSTRACT

The *KIT* exon 17 D816V mutation, which is associated with the resistance against c-Kit inhibitor and poor prognosis, frequently occurs in core binding factor acute myeloid leukemia (CBF-AML) (30%) and in mast cell neoplasms (~80%). However, the molecular basis for these effects is not fully known. To address this issue, in this study we screened molecules whose expression is altered by *KIT* D816V mutation and found that Pim kinases were overexpressed in D816V-mutant leukemic cells. To elucidate the roles of upregulated Pim kinases in D816V cells, survival kinetics, chemotaxis, and drug response assays were conducted. Collectively, our data showed that upregulated Pim kinases were involved in coordinating the proliferation, survival, migration, and drug response of the mutant cells. Further, we confirmed that upregulation of Pim kinases was a unique feature of D816V cells, compared with N822K (another c-Kit activating mutation) and N822 established by CRISPR-Cas9 genome editing. *KIT* N822K had the same proliferative advantage as D816V, but Pim kinase level was not altered.

In conclusion, our data suggest that Pim kinases could be a

promising therapeutic target in patients carrying *KIT* D816V mutation.

Keywords: Acute Myeloid Leukemia, *KIT* D816V, Pim kinase, cell survival, cell proliferation, cell migration

INTRODUCTION

c-Kit is a type III receptor tyrosine kinase (TK) expressed in hematopoietic stem cells and normally developing melanocytes, germ cells, and interstitial cells [1]. *KIT* gene alterations are detected in various cancers including acute myeloid leukemia (AML), mast cell leukemia, systemic mastocytosis, melanoma, germ cell tumors, and gastrointestinal stromal tumors, with a high frequency of mutation found in mast cell neoplasms and core binding factor (CBF)-AML. In particular, the D816V (Asp816Val) point mutation in the exon 17 TK2 region is present in up to 30% of CBF-AML cases [2,3] and up to 80% of mast cell neoplasms [4], and is linked to c-Kit inhibitor resistance and poor prognosis [5,6]. N822K (Asn822Lys), another high-frequency mutation in the TK2 domain of exon 17, is also a c-Kit activating mutation, but confers better prognosis than D816V [7]. A third c-Kit activating mutation, V560G (Val560Gly), occurs not in TK2 but in the juxtamembrane domain and confers responsiveness to c-Kit inhibitors such as imatinib [8]. These differences in therapeutic response may be attributable to the major signaling pathways that are activated by each mutation [9]. For instance, mammalian target of rapamycin (mTOR) [10], SRC kinase [11],

phosphoinositide 3-kinase (PI3K) p85 [12], and signal transducer and activator of transcription (STAT) [13] have been implicated in the survival and drug response resistance of D816V-mutant cells. However, the molecular basis for these properties is not well understood; clarifying the underlying mechanisms can provide a basis for developing novel and more effective therapeutic strategies.

Pim serine/threonine protein kinases are highly expressed in various hematologic malignancies, as well as in solid cancers, and are considered as promising therapeutic targets owing to their critical roles in cancer cells [14]. Overexpression of Pim kinases promotes cancer cell survival by regulating the cell cycle, apoptosis, and metabolism via modulation of signal transduction molecules such as mTOR [15] as well as C-X-C chemokine receptor type (CXCR) 4, which regulates the cell migration that is critical for drug response and disease relapse. Pim kinase expression is regulated by Janus kinase (JAK)/STAT, PI3K/Akt, mitogen-activated protein kinase/extracellular signal-regulated kinase (ERK), and nuclear factor (NF)-κB signaling [16]. In particular, STAT directly regulates Pim kinases expression by binding the transcription site [17] and plays a key role in the survival of cells harboring *KIT* D816V mutation.

Additionally, although the mechanism by which aberrantly

activated c-Kit affects cancer cells remains unclear, it was recently reported that Pim-1 regulates *KIT* translation [18]. Collectively, Pim kinases may be pivotal in *KIT* D816V cells in terms of cell survival, cell migration, and drug response.

The present study investigated the functional significance of *KIT* D816V mutation and Pim kinase overexpression in relation to various aggressive characteristics including cell survival, proliferation, and migration. We also compared the signal transduction pathways activated by *KIT* mutations to determine whether Pim kinase overexpression is specifically associated with D816V. Our findings indicate that Pim kinases are a promising therapeutic target in patients harboring the D816V mutation.

MATERIALS AND METHODS

1. Cell cultures

The HMC-1.1 and HMC-1.2 leukemic human mast cell lines were provided by Dr. Joseph H. Butterfield of Mayo Clinic (Rochester, MN, USA). The Kasumi-1 human AML cell line (American Type Culture Collection, Manassas, VA, USA) and the MV4-11, MOLM14, NB4, HL-60, HEL, and KG-1 leukemic cell lines were purchased from DSMZ (Braunschweig, Germany).

HMC-1 cells were cultured in Iscove's Modified Dulbecco's Medium (IMDM; Thermo Fisher Scientific, Waltham, MA, USA; 12440053). Kasumi-1 cells were cultured in Roswell Park Memorial Institute (RPMI)1640 medium (Welgene, Gyeongsan, South Korea; LM011-51), as were the other cell lines (LM011-01). All culture media were supplemented with 10%–20% heat-inactivated fetal bovine serum (Thermo Fisher Scientific; 16000044) and 1% PenStrep (Thermo Fisher Scientific; 15140122). Cells were passaged every 2–4 days.

2. DNA extraction and SNP sequencing

DNA was extracted using QIAamp DNA Mini Kit (Qiagen, Hilden,

Germany) according to the manufacturer's protocol. SNP sequencing was performed by Macrogen (Seoul, Korea) and data were analyzed using Chromas v.2.6.6 software (Technelysium, Brisbane, Australia).

3. Western blotting

Cells were incubated in protein lysis buffer (Kinexus Bioinformatics Corp, Vancouver, Canada) for 2 h on ice (per manufacturer's protocol), and then centrifuged for 25 min x 13,000 rpm at 4° C. Proteins were quantified by a Micro BCA Protein Assay kit (Thermo Fisher Scientific), loading prepared samples into 8–10% sodium dodecyl sulfate–polyacrylamide gel for electrophoretic transfer (SDS–PAGE, 2 h at 70 V) onto PVDF membranes (MilliporeSigma, Burlington, MA, USA). The membranes were blocked with 5% skim milk (GeorgiaChem, Norcross, GA, USA) and Tris–buffered saline (TBS) solution containing 5% Tween–20 (TBS/T) for 1 h at room temperature. Blots on membranes were probed, using specific primary antibodies (overnight at 4° C) and secondary antibodies diluted 1:10,000 in 1% skim milk solution. Detection was enhanced by chemiluminescence reagents.

4. Reagents and inhibitors

Human plasma fibronectin (1 mg/ml [2549971], MilliporeSigma),

dasatinib, imatinib, BKM120, taselisib, everolimus, AZD1208, PIM447, and SH-4-54 (Selleck Chemicals, Houston, TX, USA), and BLU-285 (MedChemExpress, Monmouth Junction, NJ, USA) were purchased as single agents. Cytarabine was purchased from Sigma-Aldrich.

5. Western blotting antibodies

Purchased antibodies included phospho-PI3 Kinase p85 (Tyr458)/p55 (Tyr199) (#4228), PI3 Kinase p85 (#4292), phospho-mTOR (S2481) (#2974), phospho-mTOR (S2448) (#2971), mTOR (#2972), phospho-STAT3 (S727) (#9134), phospho-STAT3 (Y705) (#9131), STAT3 (#9139), phospho-STAT5 (Y694) (#9359), STAT5 (#9363), phospho-Akt (T308) (#2965), phospho-Akt (S473) (#4060), Akt (#2920), phospho-p70S6K (T389) (#9234), phospho-4E-BP1 (Thr37/46)(#2855), phospho-p44/42 MAPK (T202/Y204) (#9101), p44/42 MAPK (T202/Y204) (#4696), Pim-2 (#4730), Pim-3 (#4165), phospho-FAK (Y576/577) (#3281), phospho-FAK (Y925) (#3284), FAK (#3285), phospho-Src (Tyr527) (#2105), Src (#2108) and α-Tubulin (#2144) (Cell Signaling Technology, Danvers, MA, USA), as well as c-Kit (sc-13508), phospho-c-Kit (Y721) (sc-101659), GAPDH (sc-25778), and Pim-1 (sc-13513) (Santa Cruz

Biotechnology, Dallas, TX, USA). Phospho-GSK3b (S9) (A00193) was purchased from GenScript (Piscataway, NJ, USA). Horseradish peroxidase-conjugated anti-rabbit and mouse secondary antibodies were also purchased (Jackson ImmunoResearch Laboratories, West Grove, PA, USA).

6. Total RNA extraction, cDNA synthesis, and quantitative Real-Time PCR

Total RNA was isolated from cultured cells with TRIzol reagent (15596018, Thermo Fisher Scientific) and NonoDrop Spectrophotometer (ND-1000, Thermo Fisher Scientific) measured the RNA concentration. Total RNA (1~5 μg) was synthesized to cDNA using RNA to cDNA EcoDry Premix (Random Hexamers) kit (639546, TaKaRa Bio Inc., Kusatsu, Japan). Real-time PCR was conducted using Applied Biosystems 7500 (Thermo Fisher Scientific) with SYBR Premix Ex Taq Ⅱ (Tli RNaseH Plus) (RR820A, TaKaRa Bio Inc.). The target mRNA level was normalized relative to 18S rRNA. The sequences of primers are listed in Table 1.

Table 1. Sequence of primer

Gene	Forward (5'-3')	Reverse (5'-3')
18S rRNA	GAACAACTGCGAAAGCATTTGC	CCTGGTAAGTTTCCCCGTGTTG
CXCR4	GGTGGTCTATGTTGGCGTCTT	TGGAGTGTGACAGCTTGGAG

7. Small interfering RNA (siRNA) transfection

Pre-designed siRNAs of *PIM1*, *PIM2*, and *PIM3* were purchased (Genolution Inc, Seoul, South Korea). Respective sequences are summarized in Table 2. Transfection was achieved using a commercial reagent (RNAiMAX Thermo Scientific Scientific) and reactivity kit (Amaxa Cell Line Nucleofector Kit V [VCA-1003] and program O-17; Lonza, Basel, Switzerland). The final concentration of siRNA was 2 μM.

Table 2. Sequence of siRNA

siRNA name			Sequence (5'-3')
1	PIM1	Sense	ACUGUUUCCUUCAUCAUGAUU
		Antisense	UCAUGAUGAAGGAAACAGUUU
2	PIM2	Sense	GUCAUUACCAGUCAUUAAAUU
		Antisense	UUUAAUGACUGGUAAUGACUU
3	PIM3	Sense	GACCUCUUCGACUUUAUCAUU
		Antisense	UGAUAAAGUCGAAGAGGUCUU
4	Negative control	Sense	CCUCGUGCCGUUCCAUCAGGUAGUU
		Antisense	CUACCUGAUGGAACGGCACGAGGUU

8. Transwell migration and invasion assay

A kit (K909-12 and K913-12; BioVision Inc, Milpitas, CA, USA) designed for cell migration/chemotaxis/invasion assay (24-well, 8-μm) was used according to the manufacturer's protocol. Cell starvation was implemented in serum-free IMDM medium for 24 h in advance.

9. Adhesion assay

We dispensed human plasma fibronectin (2.5 μg/ml) into 96-well microplates (Corning Inc, Corning, NY, USA), allowing it to harden 1 h at room temperature. Designated wells were then seeded (3 x 10^5 cells/well), incubated for 2 h at 37° C, washed in serum-free IMDM medium (300 μl) three times, and finally incubated in conditioned IMDM medium (200 μl) for 30 min at 37° C. To assess viability, a purchased solution (EZ-Cytox, 10 μl; DoGen-Bio, Seoul, South Korea) was added to each well, obtaining optical density (OD) readings at 450 nm after 2 h incubation.

10. Cell proliferation assay

Knockdown cells were seeded into 96-well plates (5,000 cells/well), measuring cellular proliferation at Days 1, 4, and 6. We added EZ-Cytox (10 μl; DoGenBio) to each well and incubated for 2

h. Proliferation was gauged by comparing OD readings at 450 nm.

11. Cell viability assay

We seeded 96-well plates (3,000 cells/well) 1 day prior to drug treatment. A total of eight drug concentrations were tested in sequential dilutions, starting at 1 or 10 μM. After 72 h of drug treatment, EZ-Cytox solution served to confirm cell viability (%), based on declines in OD readings relative to controls.

12. Outgrowth assay

HMC-1.1 and HMC-1.2 cells were cultured in T-25 flasks (Corning Inc) up to 120% and 150% confluence, using conditioned medium as previously described (see 2.1 Cell cultures).

13. Generation of *KIT* knock-in cells using CRISPR-Cas9 genome editing

Recombinant Cas9 protein, single guide RNA (sgRNA) (5' -CAAGAATGATTCTAATTATGTGG-3'), and single-strand DNA donor (ssDonor) were purchased from ToolGen, Inc. (Seoul, Korea). 1 μg sgRNA, 1 μg Cas9 protein, and 100 pM ssDonor mixture was transfected to Kasumi-1 cells using Amaxa Ⅱ electroporator (Cell Line Nucleofector Kit V [VCA-1003] and program V-001; Lonza).

After transfection, one cell per well was seeded and expanded for 2 weeks.

14. Statistical analysis

Data were compared using Student's *t*-test and two-way ANOVA with Bonferroni correction of standard software (Prism 5; GraphPad Software Inc, San Diego, CA, USA). Error bar represented mean ± SD (* $p<0.05$, ** $p<0.01$, and *** $p<0.001$).

RESULTS

1. The *KIT* D816V induces resistance to c-Kit inhibitor and differential expression of signaling molecules.

For the confirmation of the previously reported data that D816V caused resistance to c-Kit inhibitors, we performed imatinib cytotoxicity assay. HMC-1.1 cells harbor the *KIT* V560G (juxtamembrane region) mutation, whereas HMC-1.2 cells carry dual point mutations (*KIT* V560G and D816V). *KIT* single nucleotide variants (SNVs) were detected by SNP sequencing (Figure. 1A). *KIT* D816V mutant cells exhibited resistance to c-Kit inhibitor, imatinib, compared to HMC-1.1 cells (Figure. 1B).

We screened the signaling molecules to determine whether the differences in responsiveness to drug correlated with intracellular signaling pathways according to D816V mutation. We checked baseline levels of c-Kit, Akt, mTOR, STAT3, STAT5, Erk (1/2), FAK, and Src, all known to impact the metabolism of cancer cells (Figure. 1C). Activation of phospho-c-Kit was more pronounced in *KIT* D816V cells, indicating that c-Kit signaling is activated by

D816V mutation and this is perhaps one explanation for drug resistance and the poor prognosis of patients with D816V (vs. juxtamembrane domain) mutations. Expression levels of phospho-Akt (S473), phospho-Akt (T308), and Erk (1/2) were reduced in D816V mutant cells. However, phospho-mTOR (S2448), phospho-mTOR (S2481), phospho-STAT3 (S727), STAT5 (Y694), phospho-FAK (Y576/577), and phospho-Src (Y527) expression levels were increased in HMC-1.2 cells, as previously reported [19].

To determine whether these upregulated signaling molecules could affect the survival of *KIT* D816V cells, we performed cytotoxicity assay with target inhibitors (Figure. 1D). We used five target inhibitors: BKM120 and taselisib for inhibiting PI3K, everolimus for mTOR, dasatinib for Src and c-Kit, and SH-4-54 for STATs. In all inhibitors except for the STATs inhibitor, the cytotoxicity effects were 60% or more at a concentration of 1μM. Especially, everolimus treated group was more sensitive at a relatively low concentrations.

Taken together, our data showed that expression levels of signaling molecules differ with respect to D816V mutation. The expression of mTOR increased in mutant cells despite the decreased activity of Akt and Erk, which are known to activate mTOR. In addition, STATs are known to be important in D816V cells, but the

inhibitor assay has shown no reactivity. These phenomena suggest that other signaling molecules related to mTOR and STATs may be involved in D816V cells.

A.

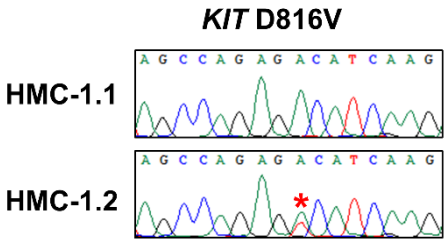
KIT D816V
HMC-1.1
HMC-1.2
A G C C A G A G A C A T C A A G
A G C C A G A G A C A T C A A G
*

B.

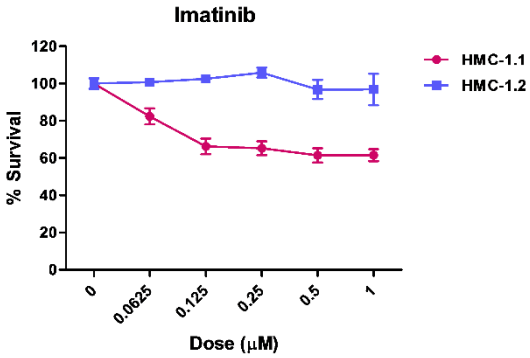
Imatinib
% Survival
120
100
80
60
40
20
0
0
0.0625
0.125
0.25
0.5
1
Dose (μM)
HMC-1.1
HMC-1.2

C.

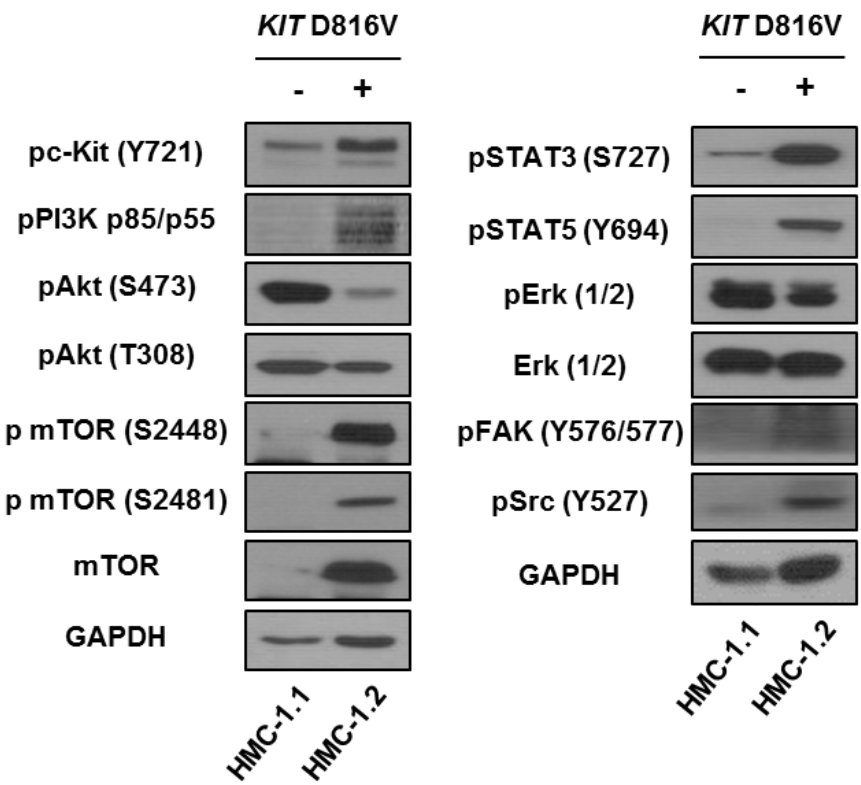
KIT D816V
- +
pc-Kit (Y721)
pPI3K p85/p55
pAkt (S473)
pAkt (T308)
p mTOR (S2448)
p mTOR (S2481)
mTOR
GAPDH
HMC-1.1
HMC-1.2
KIT D816V
- +
pSTAT3 (S727)
pSTAT5 (Y694)
pErk (1/2)
Erk (1/2)
pFAK (Y576/577)
pSrc (Y527)
GAPDH
HMC-1.1
HMC-1.2

D.

Drug	Target
BKM120	PI3K p110α/β/δ/γ
Taselisib	PI3Kα/δ/γ
Everolimus	mTOR
Dasatinib	Src, c-Kit (D816V)
SH-4-54	STAT3, STAT5

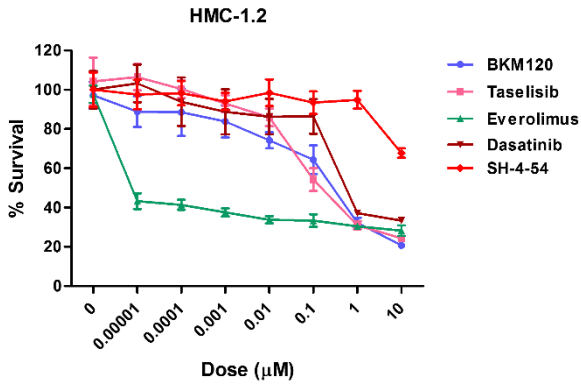

Figure 1. Screening of signaling molecules and cytotoxicity assay of *KIT* D816V cells

(A) SNP sequencing for detection of *KIT* D816V mutation. D816V mutation marked with a red star. (B) Cytotoxicity assay with imatinib in HMC-1.1 (*KIT* V560G) and HMC-1.2 (*KIT* V560G and D816V) cell lines. The drug was treated for 72 h and the % survival was calculated by measuring OD values. (C) Western blotting of signaling molecules. Phospho-c-Kit, mTOR, STATs, FAK, and Src increased in *KIT* D816V cells. (D) Cytotoxicity assay with various target drugs in D816V cells. Treatment time and calculation of % survival used the same method with (B).

2. Pim kinases upregulate in *KIT* D816V cells.

The Pim kinases, which are able to activate mTOR signaling by bypassing Akt signaling [20], and their expression is regulated by STATs. Therefore, the expression levels of Pim kinases were confirmed in order to determine whether they participate in mTOR and STATs regulation in D816V cells. The Pim kinases (Pim-1, Pim-2, and Pim-3) showed dramatic increases in *KIT* D816V cells (Figure. 2A). To confirm whether upregulation of Pim kinases is a feature unique to *KIT* D816V cells, we examined Pim kinase expression in nine human leukemic cell lines, and detected phospho-c-Kit in three *KIT* mutant cell lines—i.e., HMC-1.1, HMC-1.2, and Kasumi-1 (harboring the KIT N822K mutation). Among them, HMC-1.2 cells with *KIT* D816V showed the highest expression levels of Pim kinases. Pim-1 was expressed only in HMC-1.1 and HMC-1.2 cells but higher in HMC-1.2 cells. Pim-2 was variably expressed in all nine cell lines, with D816V cells showing the highest level Pim-3 was also variably expressed in all nine cell lines. Among those with *KIT* mutations, D816V cells showed the highest expression level (Figure. 2B).

Taken together, all Pim kinases are strongly expressed in *KIT*

D816V cells and which might play a role in the biological characteristics of the mutant cells.

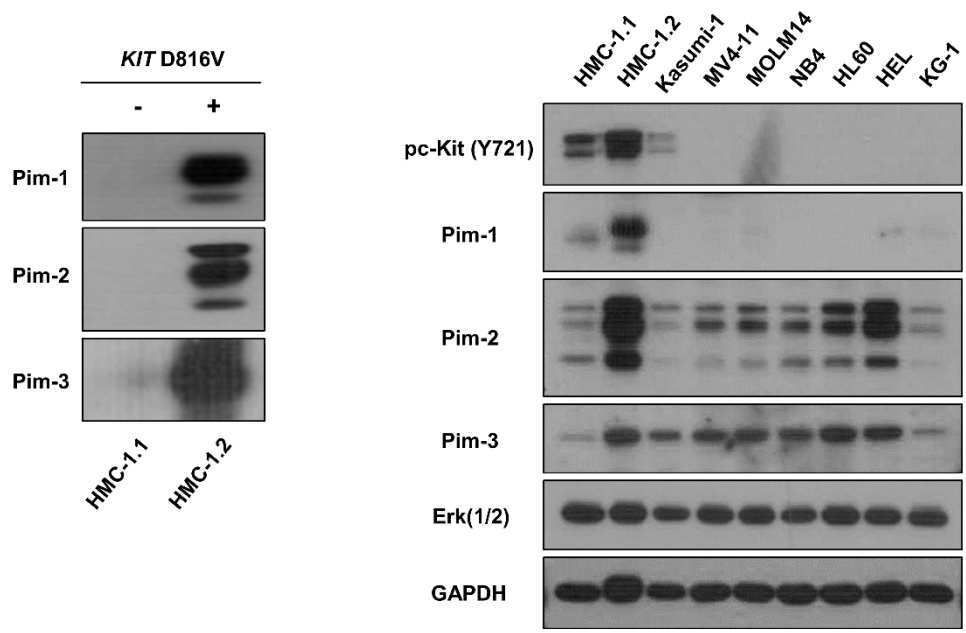

Figure 2. Pim kinases expression in various leukemic cell lines

(A) Comparison of the expression levels of Pim kinases depending on D816V mutation. (B) The expression levels of Pim kinases in nine human leukemic cell lines. Phospho-c-Kit was detected in only *KIT* mutant cell lines. Erk (1/2) served as a loading control.

3. Upregulated Pim kinases affects cell proliferation and viability of *KIT* D816V cells.

The expression of Pim kinases were downregulated using siRNAs and proliferation assay of *KIT* D816V cells was done measuring OD 1, 4, and 6 days later (Figure. 3A).

Although there were no observable changes on day 1, cell growth was markedly reduced on days 4 and 6. Cell proliferation was most strongly inhibited in siPIM all (PIM1, 2, and 3 were all knocked down). The suppression of Pim kinase expression was confirmed by western blotting (Figure. 3B).

To clarify the roles of Pim kinases and STATs in the viability of *KIT* D816V cells, we examined their expression following treatment with the c-Kit inhibitors, imatinib, dasatinib, and BLU-285. D816V cells have known resistance to imatinib [21-23] and proven reactivity to dasatinib [24] or BLU-285 [25,26]. As in the previous studies, HMC-1.2 cells responded only to dasatinib and BLU-285 (Figure. 3C), with the latter affecting cell viability at a lower concentration than the former.

Imatinib had no effect on the expression of Pim kinases and STATs or on cell viability, but these all declined upon dasatinib or

BLU-285 treatment (Figure. 3D), with the latter having a more potent effect and Pim-3 being the least affected by the drugs.

A salient feature of aggressive cancer cells is their metabolism sustained, despite the lack of environmental support [27-29]. We assessed cellular outgrowth to determine if expression levels of Pim kinases varied under such conditions with respect to *KIT* D816V mutations (Figure. 3E). Phospho-c-Kit expression increased in HMC-1.2 cells and decreased in HMC-1.1 cells as outgrowth progressed. STAT expression was unchanged or strongly increased in HMC-1.2 cells but decreased or only slightly increased in HMC-1.1 cells. Pim-1 level was downregulated in association with HMC-1.1 cell outgrowth, but the opposite trend was observed in HMC-1.2 cells. Pim-2 has three isoforms (34, 38, and 40 kDa), and one (34 kDa) of which induces apoptosis when phosphorylated at Ser112 [30] as well as cell cycle arrest at the G1 phase [31]. Expression of the 34-kDa isoform of Pim-2 in HMC-1.1 cells increased with outgrowth, implying that apoptotic signaling was activated under these conditions. In contrast, the 40- and 34-kDa isoforms were up- and downregulated, respectively, in HMC-1.2 cells, suggesting that anti-apoptotic signaling pathways were activated, instead. Pim-3 was upregulated in both cell lines but the level was higher in HMC-1.2 cells in the early phase of outgrowth. The expression of mTOR, which

is a down signaling molecule of Pim kinases and involved in cell metabolism, was also confirmed. In the case of HMC-1.2 cells, both serine 2448 and 2481 residues of mTOR showed an increase in outgrowth, but HMC-1.1 cells showed an increase only in serine 2448 residue at the end of outgrowth. The expression of p70S6K, a down signaling molecule of activated mTOR, was confirmed to be increased in only HMC-1.2 cells, even though outgrowth progressed. Meanwhile, 4E-BP1, another down signaling molecule of mTOR, was not changed in HMC-1.2 cells, but was decreased in HMC-1.1 cells. In *KIT* D816V cells, the expression of Pim kinases was increased and mTOR was activated, in a state where it was difficult to survive. To confirm that Pim kinases regulate the expression of down signaling molecule, mTOR, upstream and downstream molecules of Pim kinases were identified after treatment of Pim kinases inhibitor, AZD1208 in D816V cells (Figure. 3F). The upstream molecules of Pim kinases, c-Kit and STATs did not change, but the expression levels of mTOR, p70S6K, and 4E-BP1 in the downstream molecules were decreased with the drug treatment.

Taken together, Pim kinases regulate the cell proliferation and *KIT* D816V-mutated cells had a survival advantage even in adverse conditions via induction of phospho-STAT5 and Pim kinases. Further, induced Pim kinases enhanced cell metabolism-related signaling

transduction such as mTOR and p70S6K.

A.

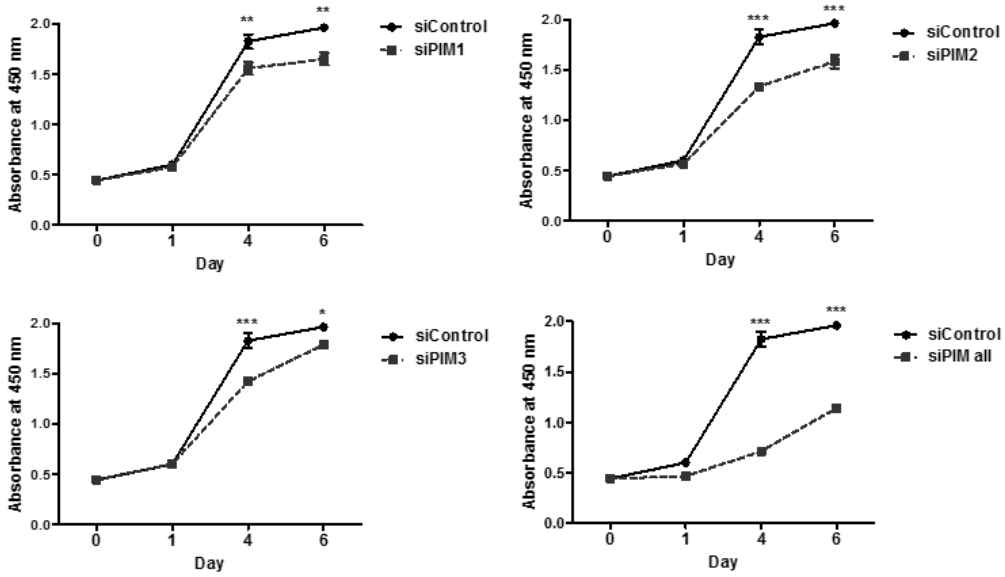
Absorbance at 450 nm
Day
siControl
siPIM1
siPIM2
siPIM3
siPIM all
**
***
*

B.

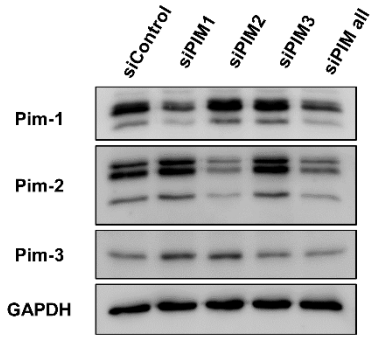
siControl
siPIM1
siPIM2
siPIM3
siPIM all
Pim-1
Pim-2
Pim-3
GAPDH

C.

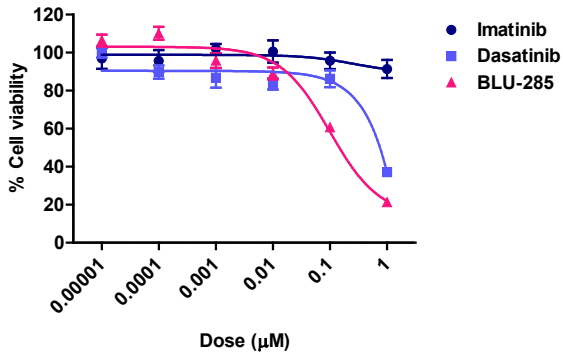
% Cell viability
Dose (μM)
Imatinib
Dasatinib
BLU-285

D.

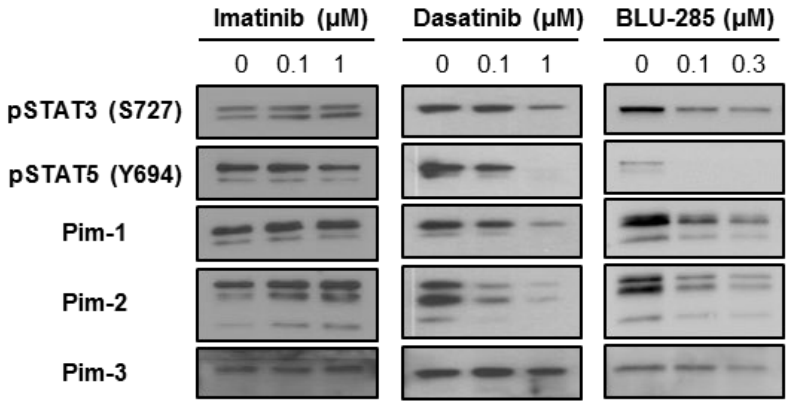
Imatinib (μM)
Dasatinib (μM)
BLU-285 (μM)
0 0.1 1
0 0.1 1
0 0.1 0.3
pSTAT3 (S727)
pSTAT5 (Y694)
Pim-1
Pim-2
Pim-3

E.

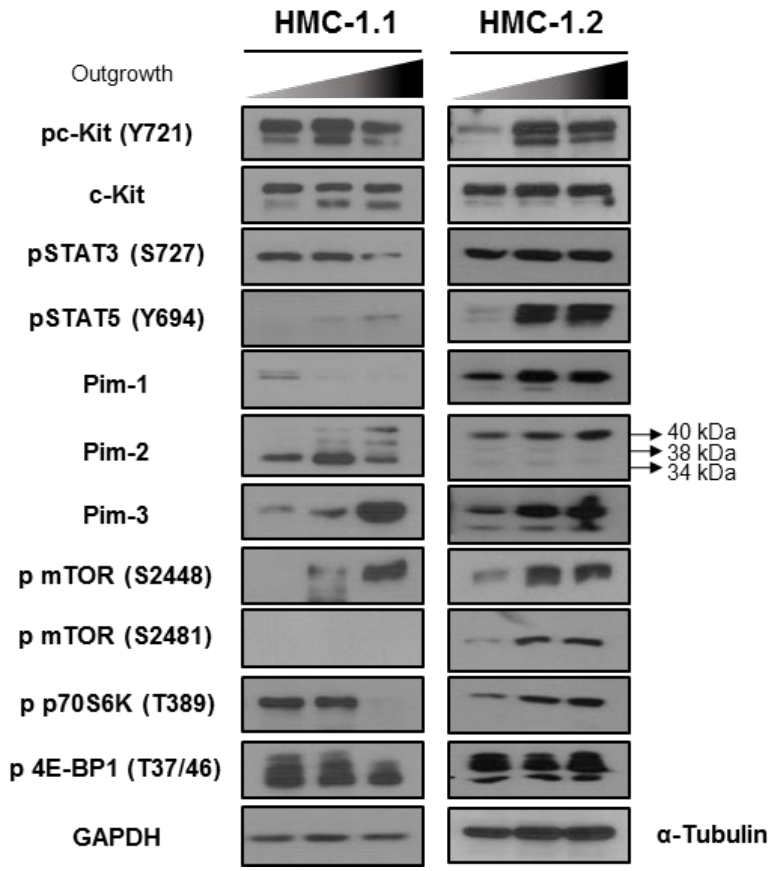
HMC-1.1
HMC-1.2
Outgrowth
pc-Kit (Y721)
c-Kit
pSTAT3 (S727)
pSTAT5 (Y694)
Pim-1
Pim-2
Pim-3
p mTOR (S2448)
p mTOR (S2481)
p p70S6K (T389)
p 4E-BP1 (T37/46)
GAPDH
40 kDa
38 kDa
34 kDa
α-Tubulin

F.

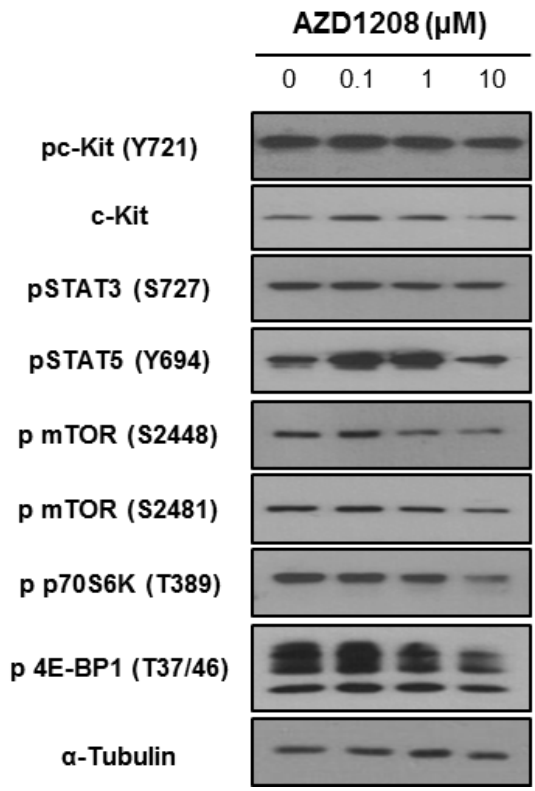
AZD1208 (μM)
0
0.1
1
10
pc-Kit (Y721)
c-Kit
pSTAT3 (S727)
pSTAT5 (Y694)
p mTOR (S2448)
p mTOR (S2481)
p p70S6K (T389)
p 4E-BP1 (T37/46)
α-Tubulin

Figure 3. Survival kinetics of *KIT* D816V cells

(A) Proliferation assay after knockdown of Pim kinases. Seeding the same number of cells into the wells and recording OD at days 1, 4, and 6. (B) Knockdown of Pim kinases was confirmed by western blotting. (C) Cytotoxicity assay of c-Kit inhibitors in D816V cells. Dasatinib and BLU-285 impair the viability of *KIT* D816V cells. (D) Expression levels of Pim kinases, STAT3, and STAT5 were decreased after dasatinib or BLU-285 drug treatment. (E) Signal transduction of HMC-1.1 and HMC-1.2 cells during outgrowth. Phosphorylation of c-Kit (Y721), STAT5, Pim kinases, and mTOR was significantly induced in *KIT* D816V cells. (F) Screening of upstream and downstream molecules of Pim kinases in D816V cells after treatment of AZD1208 for 24 h.

4. Upregulated Pim kinases activate migration ability of *KIT* D816V cells.

Cell migration and adhesion are important features of malignant cancers and are associated with CXCR4 activation by Pim kinases [32,33]. We examined whether *CXCR4* expression changes according to *KIT* D816V mutation status and found that relative *CXCR4* mRNA level was almost two-fold higher in *KIT* D816V cells (Figure. 4A).

To evaluate whether migration and adhesion capacity was changed by increased expression of Pim kinases and *CXCR4* in D816V cells, transwell migration assay and fibronectin adhesion assay were performed. *KIT* D816V cells exhibited a significantly greater capacity to migrate than did HMC-1.1 cells (Figure. 4B) and the number of migrating cells significantly declined upon knockdown of Pim kinases (Figure. 4C). Mobility of D816V cells consistently decreased almost two-fold with a Pim kinases inhibitor, PIM447, treatment for 24 h (Figure. 4D). However, adhesion ability showed no apparent alteration in D816V cells (Figure. 4E), and it was also unaffected by knockdown of Pim kinases (Figure. 4F).

Collectively, the activated migration which is related to poor prognosis by inducing a drug resistance and recurrence of D816V

cells was regulated by Pim kinases suggesting that regulation of Pim kinases could be a therapeutic strategy in patients with this mutation.

A.

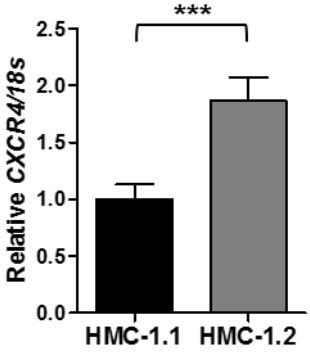
***
Relative CXCR4/18s
2.5
2.0
1.5
1.0
0.5
0.0
HMC-1.1
HMC-1.2

B.

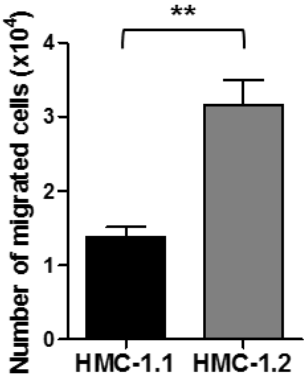
**
Number of migrated cells (x10^4)
4
3
2
1
0
HMC-1.1
HMC-1.2

C.

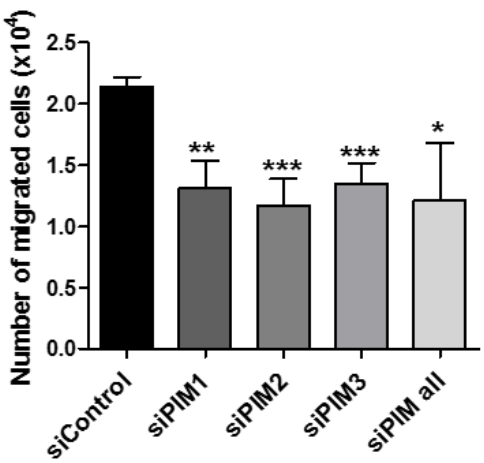
Number of migrated cells (x10^4)
2.5
2.0
1.5
1.0
0.5
0.0
**
***
***
*
siControl
siPIM1
siPIM2
siPIM3
siPIM all

D.

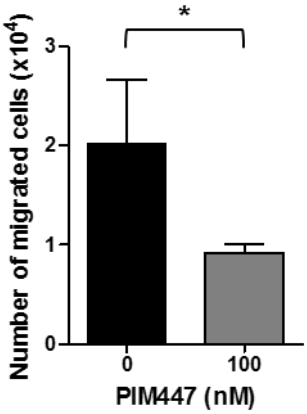
*
Number of migrated cells (x10^4)
3
2
1
0
0
100
PIM447 (nM)

E.

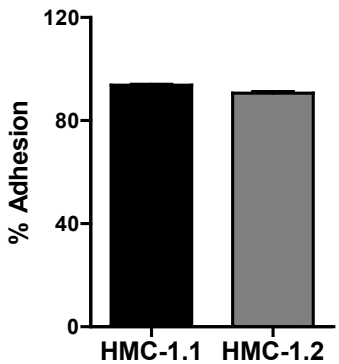
% Adhesion
120
80
40
0
HMC-1.1
HMC-1.2

F.

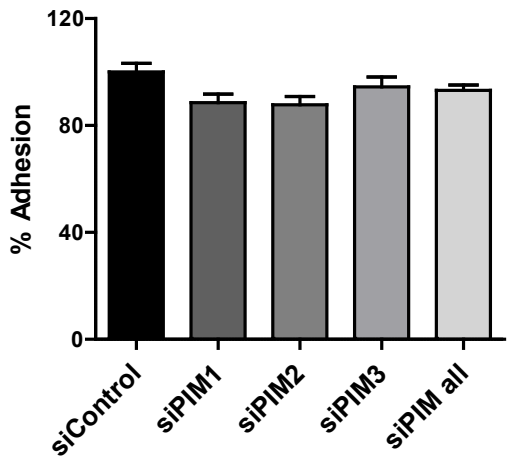
% Adhesion
120
80
40
0
siControl
siPIM1
siPIM2
siPIM3
siPIM all

Figure 4. Cell migration and adhesion assay

(A) Relative expression of *CXCR4* according to D816V mutation. (B) Transwell migration assay was used for evaluating cellular mobility by the mutation. (C, D) The relationship between expression of Pim kinase and cellular mobility was confirmed by transfection of siRNA and treatment of Pim kinase inhibitor. All migration assay was conducted using a transwell chamber. Seeding the cells into the top chamber and quantifying migrated cells after 24 h. (E) Fibronectin-binding assay exploring the capacity for cell adhesion ability according to the mutation and (F) Pim kinases.

5. In contrast to *KIT* D816V cells, N822K cells respond to the c-Kit inhibitor, imatinib.

In order to identify the characteristics of D816V cells having a clinically worse prognosis when compared with the c-Kit activating mutation, N822K, occurring in the same TK2 domain, a cytotoxicity assay was performed on N822K cells with imatinib that is already not effective in D816V cells. *KIT* N822K cells were more sensitive to imatinib compared to D816V cells (Figure. 5A). The IC_{50} values of N822K cells were around 1 μM.

To confirm the signal transduction effect of imatinib on N822K cells, western blotting was performed after imatinib treatment. Phospho-c-Kit and Pim-3 were downregulated by as low as 1 μM concentration of imatinib. Akt related signaling molecule, GSK3b also was decreased. Expression of mTOR and their down signaling molecule, p70S6K, were also decreased by imatinib (Figure. 5B).

Taken together, *KIT* N822K cells had a differential response to imatinib. It is necessary to confirm whether these differences are related to the effect of upregulated Pim kinases in D816V cells.

A.

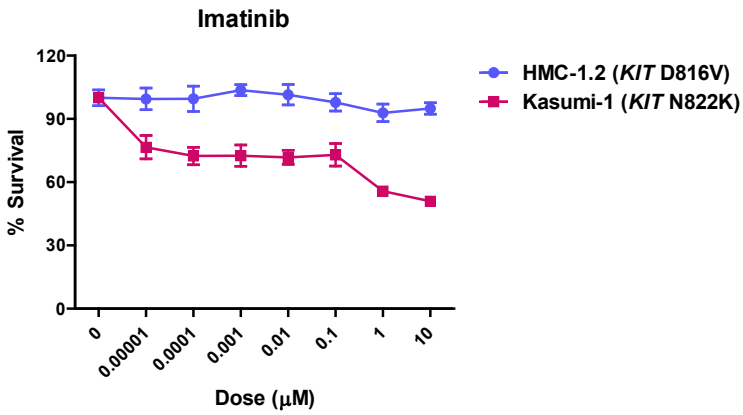

B.

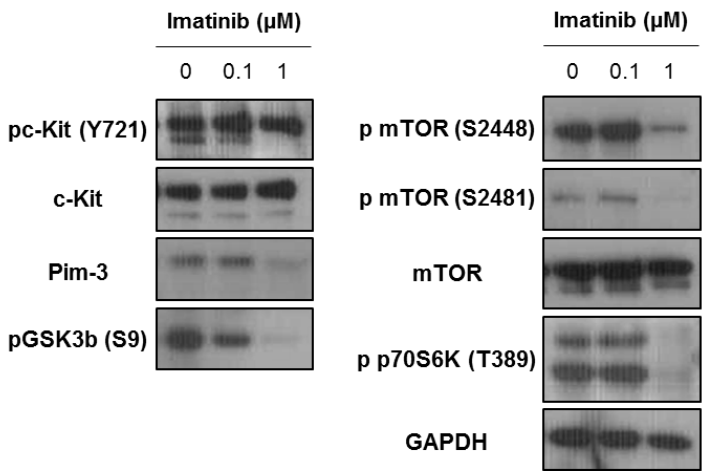

Figure 5. Effect of c-Kit inhibitor, imatinib on *KIT* N822K cells

(A) Comparison of cytotoxicity effects of imatinib on *KIT* D816V and N822K cells. The drug was treated for 72 h and then cytotoxicity effects were evaluated by measuring OD values. (B) Signal transduction of *KIT* N822K cells after treatment of imatinib. GAPDH was used as a loading control.

6. Upregulated Pim kinases is a specific characteristic of *KIT* D816V cells

To confirm whether the D816V mutation with clinically worse prognosis is associated with upregulated Pim kinases when compared to N822K, the mutation was replaced with a wild-type sequence by CRISPR-Cas9 genome editing in AML cells with N822K mutation (Kasumi-1) (Figure. 7A) and then knock-in was confirmed by SNP sequencing (marked with a red star).

To evaluate the proliferation effect of *KIT* N822K, we conducted a proliferation assay. Compared to *KIT* N822K cells, *KIT* wild-type clone # 8 had decreased proliferative ability (Figure. 7B). Transwell migration assay, basement membrane invasion assay, and fibronectin adhesion assay were conducted to assess the chemotaxis ability to determine whether the highly migrative feature in D816V cells occur similarly in N822K cells. Similar to D816V cells, N822K had increased migration ability (Figure. 7C). N822K cells had a slightly increased invasion ability than *KIT* wild-type cells (Figure. 7D) and there was no difference in adhesion ability by the *KIT* mutation (Figure. 7E).

Ultimately, to investigate whether the upregulated Pim kinases

was a specific characteristic of D816V cells, we screened the downstream signal transduction pathway of c-Kit (Figure. 7F). *KIT* wild-type clone #8 had decreased expression of phospho-c-Kit and total c-Kit. Adjustment of expression of PI3K, Erk (1/2), mTOR, FAK and Src were same as in D816V cells. However, Akt expression was opposite to that of D816V cells. Pim-3 and STAT3 (phospho-STAT5 was not detected) expressions were not changed by the *KIT* N822K mutation.

Taken together, *KIT* N822K cells, just like in D816V cells, activated mobile and proliferative ability compared to wild-type. Expressions of PI3K p85, mTOR, FAK and Src in signal transduction were similar to those of D816V cells. However, the expression of Pim and STATs was not altered by the N822K mutation. These characteristics in signal transduction may be related to the fact that patients with D816V have a worse prognosis than N822K.

A.

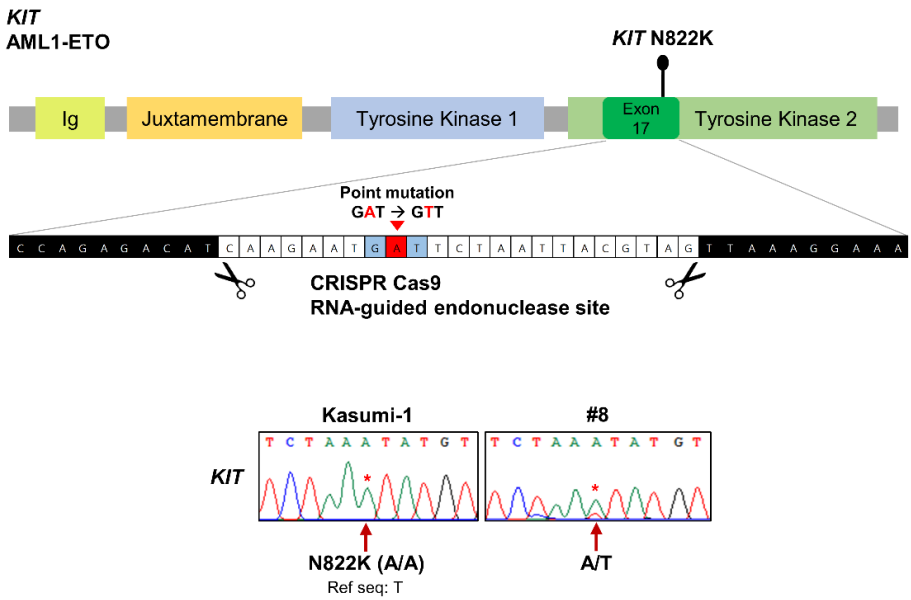
KIT
AML1-ETO
KIT N822K
Ig
Juxtamembrane
Tyrosine Kinase 1
Exon 17
Tyrosine Kinase 2
Point mutation
GAT → GTT
CRISPR Cas9
RNA-guided endonuclease site
Kasumi-1
#8
KIT
N822K (A/A)
Ref seq: T
A/T

B.

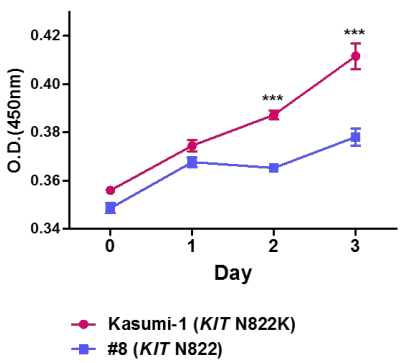
O.D.(450nm)
Day
Kasumi-1 (KIT N822K)
#8 (KIT N822)

C.

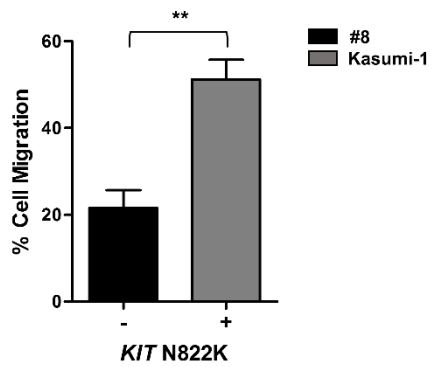
% Cell Migration
#8
Kasumi-1
KIT N822K

D.

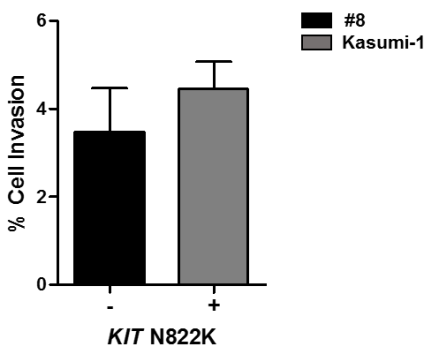
% Cell Invasion
#8
Kasumi-1
KIT N822K

E.

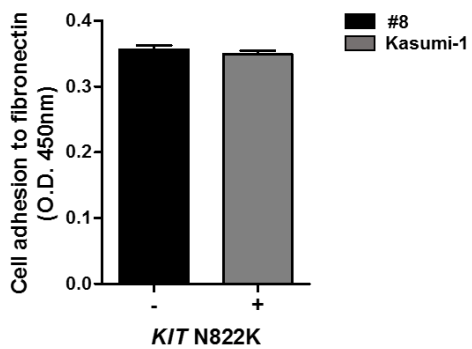
Cell adhesion to fibronectin (O.D. 450nm)
#8
Kasumi-1
KIT N822K

F.

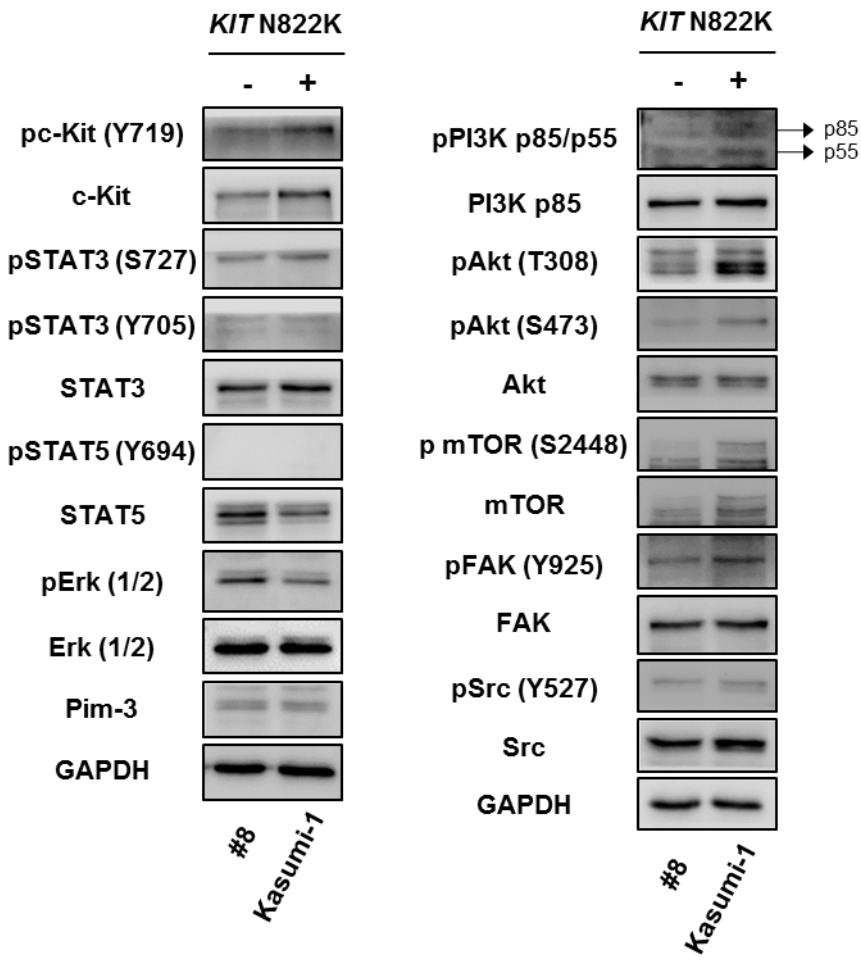
KIT N822K
- +
pc-Kit (Y719)
c-Kit
pSTAT3 (S727)
pSTAT3 (Y705)
STAT3
pSTAT5 (Y694)
STAT5
pErk (1/2)
Erk (1/2)
Pim-3
GAPDH
#8
Kasumi-1
KIT N822K
- +
pPI3K p85/p55
p85
p55
PI3K p85
pAkt (T308)
pAkt (S473)
Akt
p mTOR (S2448)
mTOR
pFAK (Y925)
FAK
pSrc (Y527)
Src
GAPDH
#8
Kasumi-1

Figure 6. Effects of *KIT* N822K mutation on leukemic cells

(A) Schematic representation of *KIT* N822K knock-in (KI) to replace the mutation with wild type using CRISPR-Cas9 genome editing and confirmed the KI by SNP sequencing. #8 was a KI clone (mutation was marked with a red star). (B) Proliferation assay of KI cells for 3 days. Proliferation was calculated by measuring OD values for 3 days. Transwell migration assay(C), invasion assay(D), and fibronectin adhesion assay(E) were used to evaluate chemotaxis ability of KI clone. Only migration ability showed a significant difference according to the mutation. (F) Screening of signal transduction according to *KIT* N822K mutation. Expressions of phospho-c-Kit, PI3K p85/p55, Akt, mTOR, FAK, and Src were increased by N822K mutation.

7. Downregulated Pim kinases increase the response to c-Kit inhibitor and cytarabine in *KIT* D816V cells

In order to confirm the effects of upregulated Pim kinases in D816V cells on drug response, a c-Kit inhibitor, BLU-285, and a well-known chemotherapeutic agent, cytarabine, were used to Pim kinases knockdown cells (Figure. 7). Both drugs were more effective in Pim kinases knockdown cells. In particular, siPIM all (knockdown of PIM1, 2, and 3) cells were most sentive. BLU-285 was put for 72 h at 100 nM concentration. Among the Pim kinase alone knockdown cells, siPIM1 cells were most sensitive among single KI cells (Figure. 7A). Nevertheless, siPIM all cells showed a greatest response which was almost two-fold higher than siPIM1 cells. Cytarabine was placed for 120 h at 500 nM concentration. Similar to the BLU-285 treatment group, siPIM1 cells showed the highest reactivity in the single knockdown group and siPIM all cells showed about 5 times higher drug response than the control group (Figure. 7B).

These data suggest that modulation of Pim kinase in D816V cells could influence the response to therapeutic agents.

A. B.

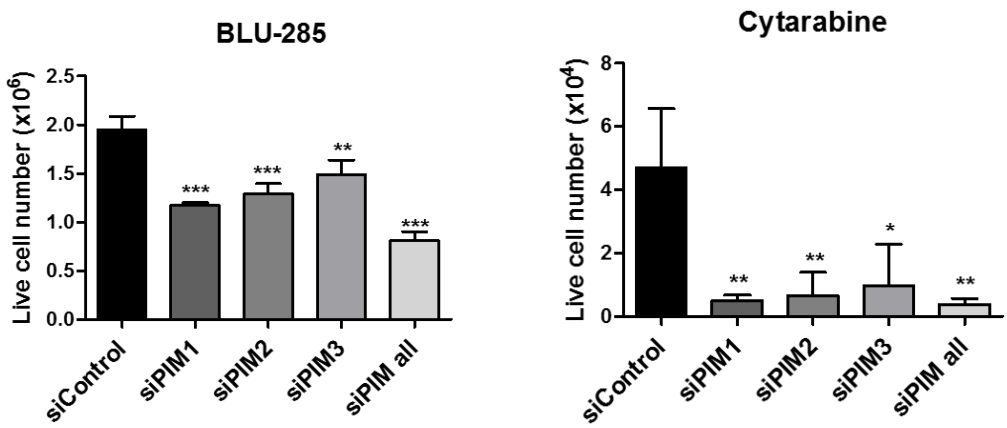

Figure 7. Evaluation of drug response after downregulated Pim kinases

(A)The response to BLU-285 (c-Kit inhibitor) and (B) cytarabine (chemotherapy agent) in Pim kinases downregulated cells. siRNA transfected cells were seeded at $1.07x10^5$ cells into 24-well plates. BLU-285 (100 nM) was placed for 72h and cytarabine (500 nM) for 120h.

Table 3. Expression of *PIM* in TCGA AML samples (n=165, PanCancer Atlas)

Patient ID	CBF-AML	*KIT* alteration	*PIM1*	*PIM2*	*PIM3*
TCGA-AB-2937	AML1-ETO	D816V	HIGH		
TCGA-AB-2939		D816V	HIGH		
TCGA-AB-2881	AML1-ETO	D816Y			
TCGA-AB-2806		HIGH			
TCGA-AB-2849		HIGH			
TCGA-AB-2867		HIGH			
TCGA-AB-2874		HIGH			
TCGA-AB-2882		HIGH			
TCGA-AB-2889	CBFB-MYH11	HIGH			

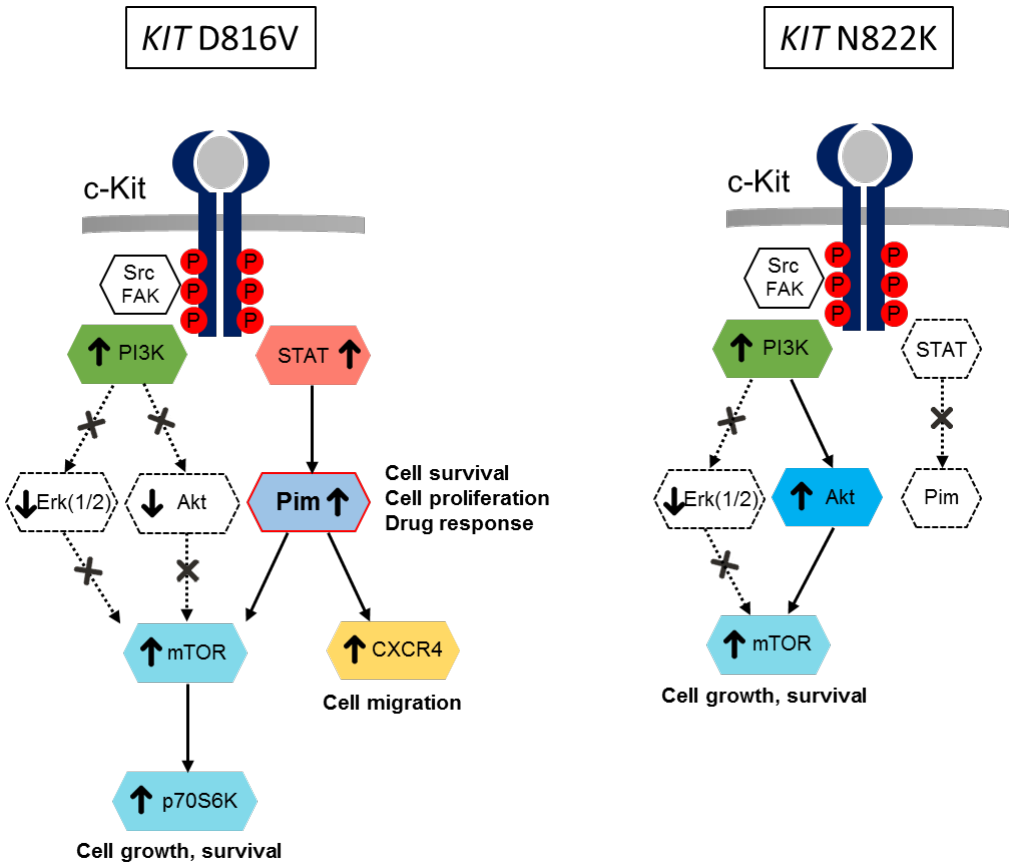

Figure 8. Summary of signal transduction cascades associated with *KIT* D816V and N822K mutations

DISCUSSION

The *KIT* D816V mutation in mast cell neoplasms occurs at a very high rate (> 80%) and in AML1-ETO fusion AML patients, at approximately 30%. The mutation significantly impacts patient prognosis depending on overall mutation burden [6]. Thus, therapeutic strategies that target D816V cells have potential clinical benefits and are currently being explored in clinical trials.

Drugs targeting D816V cells are classified as agents that regulate c-Kit receptor activation or as multi-TK inhibitors (TKIs) that act on a broad spectrum of TKs including c-Kit. Cells harboring D816V are inherently resistant to the c-Kit inhibitor, imatinib. Masitinib, which also targets c-Kit, has recently been tested in clinical trials, and BLU-285 trials are actively ongoing. Ponatinib [21] and dasatinib [24] are multi-TKIs that exploit signaling molecules other than c-Kit to regulate D816V cells. Indeed, these agents alter the survival of D816V cells via STAT5 and Src regulation. Thus, targeting different factors that are upregulated in this context is likely to be more effective than c-Kit receptor blockade alone.

A study of SM patients with D816V mutation showed that a high proportion of them shown upregulation of *PIM1* [34], implying that Pim

kinases play a biologically important role in this disease. In the TCGA AML data published on cBioPortal(n=165, PanCancer Atlas), the expression of *PIM1* was increased in all patients with *KIT* D816V mutation regardless of CBF-AML subtypes. On the other hand, *PIM* expression was not altered in a patient with *KIT* D816Y + CBFB-MYH11. In addition, there was no alteration in *PIM* expression in patients with *KIT* overexpression. Overall, the overexpression of *PIM* (*PIM1*) is observed only in patients with *KIT* D816V mutation (Table 3). With our results, regulation of Pim kinases could also be a candidate for treating of D816V cells just like STATs and Src which are already utilized as therapeutic targets.

Given their important roles in the progression of hematologic and solid cancers, and clinical trials of new drugs targeting Pim kinases are currently being conducted. Most of these are pan-Pim kinase inhibitors that act on Pim-1, -2, and -3 and are predicted to have potent anti-cancer effects. Indeed, in our proliferation assay, the greatest degree of inhibition was observed by suppressing all three proteins. In a study of the pan-Pim kinase inhibitor, AZD1208, on AML cell lines, showed that drug response correlates with Pim-1 and STAT5 expression and AZD1208 induces cell death by decreasing 4E-BP1 and p70S6K activation [35]. A phase I trial for AZD1208 has been completed in advanced solid tumors and malignant

lymphomas and a clinical trial for another pan-Pim kinase inhibitor, PIM447, combined with the JAK1/2 inhibitor, ruxolitinib and cyclin-dependent kinase 4/6 inhibitor, LEE011, is ongoing. Combination treatment with an inhibitor of JAK1/2, which is associated with the alteration of STAT activity, is especially promising as demonstrated by the results of the present study.

Precision medicine improves treatment outcome by targeting the specific factors promoting cancer cell survival in a patient. It is therefore important to identify the main signaling molecules involved in cancer cell survival and clarify their functions. We determined that Pim kinases are overexpressed in *KIT* D816V cells and described their functions in cancer. Pim-2 was the most highly expressed, followed by Pim-1 and -3; when Pim-2 was removed by knock-down, cell proliferation was most inhibited on day 6 compared to Pim-1 and 3. In contrast, Pim-3 was least affected by drug treatment and thus, leading to the lowest degree of growth inhibition on day 6. Thus, the function of each Pim molecule in *KIT* D816V cells is related to its expression level, with Pim-2 being the most important in terms of the survival of *KIT* D816V cells.

Various non-canonical pathways are known to be involved in cell survival [36] and tumorigenesis [37]. In other words, some cells mainly use a non-canonical pathway rather than canonical signal cascade. In

order to properly control the cells that use the non-canonical pathway as the main signaling cascade, it is important to discover and control the molecules of the non-canonical pathway in addition to targeting the canonical signaling molecules. We found that D816V cells used Pim kinases rather than Akt or Erk(1/2) to activate the down signal transduction pathways such as mTOR (PI3K-STATs-Pim kinases-mTOR). However, N822K cells used the canonical signaling cascade (PI3K-Akt-mTOR) for activating the downstream signaling pathway (Figure. 8). Such a non-canonical pathway as shown in D816V cells is unusual and this feature may be associated with poor prognosis than other c-Kit activating mutations.

Collectively, our data showed that Pim kinases are overexpressed in *KIT* D816V cells, altering their viability and survival through proliferative and migratory advantages. Further, we figure out that upregulated Pim kinases was a unique characteristic of D816V cell compared with the same c-Kit activating mutation, N822K.

The results of this study demonstrate that Pim kinase overexpression is associated with *KIT* D816V mutation, which is frequently detected in CBF-AML and results in poor prognosis. Given their critical role in cancer cell survival, migration, and drug response, Pim kinases are promising therapeutic targets in patients

with *KIT* D816V.

Ⅱ. A novel truncation mutation, *MYH8* R1292X in AML, induces morphological change, cell migration, and epithelial to mesenchymal transition via Raf/MAPK pathway

ABSTRACT

MYH8 is an actin-based motor protein involved in integrin-mediated cell adhesion and migration. However, the association of *MYH8* mutation and cancer is unclear. In this study, I investigated the biologic significance of novel *MYH8* tail truncation mutation, R1292X in acute myeloid leukemia (AML) by whole-exome sequencing (WES) and targeted re-sequencing of 209 AML patients. The patients harboring the mutation all relapsed within 3.8-20.9 months. To explore the functional consequence of the mutation in AML progress, we established knock-in cell lines using CRISPR-Cas9 genome editing. Using the established mutant model, we assessed the features of cancer progress. The mutant cells had improved motility that was confirmed by immunofluorescence staining, wound healing, and adhesion assay. The cell morphology and cell cycle were altered to facilitate migration and epithelial to mesenchymal transition (EMT) transcription factors also were increased. The Raf and p44/42 MAPK pathway was a major regulator of these characteristics proved by screening of signal transduction pathway and inhibitor assay. Further, a public cancer genome database (cBioPortal) shows that *MYH8* tail truncation mutations occurring near the R1292 position of the

genome may have a significant function in cancer. In conclusion, truncation of *MYH8* may be related to AML progress by inducing increased cell migration and EMT features and inhibition of the Raf/MAPK pathway would be a therapeutic strategy for AML patient with *MYH8* tail truncation.

Keywords: Acute Myeloid Leukemia, Next-Generation Sequencing, *MYH8*, Truncation mutation, Epithelial-Mesenchymal Transition, cell migration

INTRODUCTION

As genomic studies have progressed, pathogenic gene mutations associated with various cancers have been reported. Acute myeloid leukemia (AML) develops due to genetic alterations in undifferentiated cells such as myeloid stem cells and myeloblasts. Mutations in *NPM1, FLT3, DNMT3A, CEBPA, IDH1/2, and RUNX1* are well-defined cancer drivers in AML [38]. Except for these important genetic factors, mutations with unknown function account for 10% of the total genetic aberration [39]. Hence, functional studies of these unknown mutations are needed to fully understand the AML pathophysiology.

Meanwhile, the correlation between myosin gene alterations and tumor biology remains controversial. While myosin has no correlation with tumors in general, some myosins are reported to be involved in cancer. Myosins are reported to function as tumor suppressors or activators depending on the specific myosin and cancer type [40]. *MYO1A* acts as a tumor suppressor in colorectal [41] and gastric tumors [42]. *MYH9* exerts tumor-suppressing function in squamous cell carcinoma and other cancers [43]. MYO6 is overexpressed in ovarian and prostate cancers, and overexpression of MYO6 increases the

migration ability of cancer cells [44,45]. Similarly, overexpression of MYO10 is observed in aggressive breast cancer and leads to increased invasiveness and poor prognosis [46]. Among the myosins, the function of *MYH8* in cancer is not well known. MYH8 is an actin-based motor protein involved in skeletal muscle contraction [47] and integrin-mediated cell adhesion and migration [48]. Together with *MYH3* and *MYL4*, *MYH8* is a developmental myosin, a type of myosin that is temporarily expressed in the fetal and embryonic stages and rapidly diminishes in adult cells [49,50]. So far, the pseudocamptodactyly syndrome is the only reported disease associated with *MYH8* gene alteration [51]. As with other myosins, *MYH8* might have functions in cancer that have not yet been revealed. Therefore, it is important to study its mechanism to elucidate its effects on cancer cells.

On the other hand, the epithelial-mesenchymal transition (EMT) is a cellular process that promotes metastasis and poor prognosis by increasing tumor cell migration and invasiveness in many solid tumors [52]. Several transcription factors (TFs), including *SNAIL*, *SLUG*, *TWIST*, and *ZEB1/2,* modulate the EMT and are related to drug resistance and cancer stemness [53,54]. Recently, the role of these EMT factors in hematologic malignancies has been reported: upregulation of EMT TFs is associated with invasiveness, cancer stemness, and drug resistance, which, in turn, affects cancer

prognosis [55–57]. The intracellular signaling molecules regulating EMT are TGF-β [58–60], PI3K-Akt [61,62], JAK-STATs [63], and RAS-MAPK [64], depending on cell and disease type. These pathways are therapeutic targets because of their ability to control EMT. Activation of cell migration is one of the EMT features regulated by integrin-mediated migration and adhesion process. Therefore, *MYH8* mutations have a chance to modify cell migration, adhesion, and EMT molecules. However, the correlations of *MYH8* mutation and EMT remain unclear.

This study is focused on identifying the functions of the *MYH8* truncating mutation, R1292X that we found through Next-Generation Sequencing (NGS) on cells. We constructed *MYH8*-mutated cell lines using the CRISPR-Cas9 genome editing system. Using these established cell lines, we examined whether *MYH8* R1292X affects cancer progress properties including cell migration, morphology, proliferation, and EMT features such as the levels of N-cadherin, vimentin, Zeb1, Slug, and Snail. We also investigated the cellular signaling pathway involved in the features caused by this mutation.

MATERIALS AND METHODS

1. Patient samples and genomic DNA extraction

The adult AML patient samples used in this study were collected with informed consent from patients at the Seoul National University Hospital. For WES, 53 paired samples of germline controls and tumors were used. We performed targeted re-sequencing to identify the somatic mutation found in WES in 156 tumor samples from the AML patient cohort. Saliva DNA was used for germline control. All tumor samples were taken from bone marrow at diagnosis and saliva samples were collected at complete remission in a saliva DNA collection tube (Norgen Biotek, ON, Canada). QuickGene DNA whole blood kit S (Kurabo Industries Ltd., Osaka, Japan) and Qiagen DNeasy kit (Qiagen, Hilden, Germany) were used for genomic DNA extraction.

2. NGS study for the discovery of a novel mutation in AML

WES was performed with the Solexa sequencing technology platform (HiSeq2000, Illumina, San Diego, CA, USA). For capturing the target exons, SureSelect Human All Exons V3 and V5 probe sets (Agilent, Santa Clara, CA, USA) were used for hybridizing with 200-

250 bp of purified DNA following the manufacturer's protocol. The Burrows-Wheeler Aligner (BWA-0.7.5) was used for alignment to the human reference genome (GRCh37). We identified somatic mutations using ADIScan [65]. All analyses were conducted using the default options. Targeted re-sequencing was performed using the Ion AmpliSeq custom panel (Thermo Fisher Scientific), and the Ion AmpliSeq Library Kit 2.0 (Thermo Fisher Scientific) was used for library construction. The Ion OneTouch System (Thermo Fisher Scientific) was used for barcoding the library and the Ion Proton Sequencer System (Thermo Fisher Scientific) was used for sequencing of the samples. After calling variants with Torrent Variant Caller (ver 4.2) (Thermo Fisher Scientific), filtering was conducted to eliminate errors (1, average depth of total coverage > 30; 2, coverage of each variant > 10; 3, variant frequency > 0.1 and $p < 0.01$).

3. *MYH8* R1292X knock-in cell line establishment

The *MYH8* R1292X knock-in (KI) cell lines were generated by ToolGen, Inc. (Seoul, Korea) using the CRISPR-Cas9 genome editing system (Clone names: #43 and #81). Gene KI has conducted in hTERT RPE-1 cells. *MYH8* R1292X KI was confirmed using deep sequencing (MiSeq, Illumina).

4. Cell culture

The human epithelial cell line hTERT RPE-1 was provided by Prof. Hyunsook Lee from Seoul National University, Institute of Molecular Biology and Genetics (Seoul, Korea). hTERT RPE-1, *MYH8* KI #43, and *MYH8* KI #81 cells were cultured in DMEM:F-12 1:1 mixture (1X) medium (LM002-04, WELGENE Inc., Gyeongsan, Korea) supplemented with 10% heat-inactivated fetal bovine serum (16000044, Thermo Fisher Scientific), 2.5 mM L-glutamine, 15 mM HEPES, and 1% penicillin-streptomycin (10000 U/ml) (15140122, Thermo Fisher Scientific) and passaged every 2-3 days. The cells were incubated in a highly humidified atmosphere of 5% CO_2 and 95% air at 37° C.

5. Proliferation assay

hTERT RPE-1, *MYH8* KI #43, and *MYH8* KI #81 cells were counted using Countess II FL Automated Cell Counter (Thermo Fisher Scientific) and $3x10^3$ cells/well were seeded in 96-well plates (3598, Corning, Corning, NY, USA) for 1~3 days. Cell proliferation was confirmed using the EZ-cytox cell viability assay kit (EZ-BULK150, DAEILLAB Service Co., Seoul, Korea) for 3 h and then OD was measured at 450 nm.

6. Cell cycle assay

$1x10^6$ cells were prepared and washed with DPBS. The cell pellets were re-suspended with 300 μl fresh DPBS. 700 μl of cold ethanol was slowly added during vortexing to fix the cells and the cells were incubated for 1 h at −20 ℃. After incubation, the cells were spinned down at 13,000 rpm for 5 min to remove ethanol and then washed with cold DPBS. Cell pellets were resuspended in 100 μl DPBS and 2μl of RNase A was added (A7973, Promega, WI, USA). Then, the cells were incubated for 1 h at room temperature. 5 μl PI solution (556463, BD Pharmingen, CA, USA) was added and the cells were analyzed using flow cytometry (BD FACSCANTO II, CA, USA) at 488 nm.

7. Total RNA extraction, cDNA synthesis, and quantitative Real-Time PCR

Total RNA was isolated from cultured cells with TRIzol reagent (15596018, Thermo Fisher Scientific) and Eppendorf BioSpectrometers (6137000901, Eppendorf, Hamburg, Germany) measured the RNA concentration. Total RNA (2 μg) was synthesized to cDNA using RNA to cDNA EcoDry Premix (Random Hexamers) kit (639546, TaKaRa Bio Inc., Kusatsu, Japan). Real-time PCR was conducted using Applied Biosystems 7500 (Thermo Fisher Scientific)

with SYBR Premix Ex Taq Ⅱ (Tli RNaseH Plus) (RR820A, TaKaRa Bio Inc.). The target mRNA level was normalized relative to 18S rRNA. The sequences of primers are listed in Table 1.

Table 1. Sequence of primer

Gene	Forward (5'-3')	Reverse (5'-3')
MYH8	CACGCTGGATGCAGAGATTA	TCAGGATTCCTTGGGTGTTC
18S rRNA	GAACAACTGCGAAAGCATTTGC	CCTGGTAAGTTTCCCCGTGTTG
MMP1	GATGTGGAGTGCCTGATGTG	TGCTTGACCCTCAGAGACCT
MMP2	ATGACAGCTGCACCACTGAG	ATTTGTTGCCCAGGAAAGTG
MMP3	TCATTTTGGCCATCTCTTCC	GGGAAACCTAGGGTGTGGAT
MMP7	GAGTGCCAGATGTTGCAGAA	AAATGCAGGGGGATCTCTTT
MMP9	GTGAGTTCCCGGAGTGAGTT	CACTCCTCCCTTTCCTCCAG
MMP11	GTCTTGGTAGGTGCCTGCAT	CCTGGGACAGGATTGAGGTA
MMP12	ACACATTTCGCCTCTCTGCT	CCTTCAGCCAGAAGAACCTG
MMP13	AACATCCAAAAACGCCAGAC	GGAAGTTCTGGCCAAAATGA

8. Western blotting

Cells were washed using cold Dulbecco's Phosphate-Buffered Saline (DPBS) (LB001-02, WELGENE). Cell pellets were lysed in kinexus protein lysis buffer (protocol is described at http://www.kinexus.ca/) for 2 h on ice. Then, the cells were centrifuged for 25 min at 13,000 rpm at 4° C. Protein quantification was conducted using a Micro BCA Protein Assay kit (Thermo Fisher Scientific). Prepared protein samples were separated using 8~10%

sodium dodecyl sulfate-polyacrylamide gel electrophoresis (SDS-PAGE) and electrotransferred onto PVDF membranes (Merck Millipore, Burlington, MA, USA). The membrane was blocked with 5% skim milk and a Tris-buffered saline solution containing 5% Tween-20 (TBS/T) for 1 h at room temperature. Blots on membranes were probed with specific primary antibodies overnight at 4° C, and secondary antibodies diluted at a ratio of 1:10,000 in 1% skim milk solution were used for primary antibody detection. The detection was enhanced by chemiluminescence reagents.

9. Western blotting antibodies and inhibitor

Trametinib (GSK1120212) was purchased from Selleckchem (Houston, TX, USA). The anti-MYH8 (#PA5-72846) was purchased from Thermo Fisher Scientific. The anti-N-Cadherin (#4061), Snail (#3895), Vimentin (#5741), TCF8/ZEB1 (#3396), phospho-STAT3 (Y705) (#9145), phospho-STAT3 (S727) (#9134), STAT3 (#4904), phospho-STAT5 (Y694) (#9359), STAT5 (#9363), phospho-Akt (T308) (#2965), phospho-Akt (S473) (#4060), Akt (#2920), phospho-c-Raf (S338) (#9427), c-Raf (#9422), B-Raf (#9434), phosphor-p44/42 MAPK (T202/Y204) (#9101), p44/42 MAPK (T202/Y204) (#4696), and TGF-β (#3709) antibodies were purchased from Cell Signaling

Technology (Danvers, MA, USA). GAPDH (sc-25778), SLUG (sc-166476), and TWIST (sc-81417) antibodies were purchased from Santa Cruz Biotechnology (Dallas, TX, USA). The anti-phospho-CXCR4 (S339) (ab74012) and CXCR4 (ab2074) were from Abcam (Cambridge, UK). The horseradish peroxidase conjugated anti-rabbit and mouse secondary antibodies were purchased from Jackson ImmunoResearch (West Grove, PA, USA).

10. Immunofluorescence

$4x10^4$ cells were cultured for 2 days to poly-L-Lysine (P4707, Sigma-Aldrich, St. Louis, MO, USA) coated coverslip. The cells were fixed with 4 % formaldehyde (HT501128, Sigma-Aldrich) for 10 min. Fixed cells were washed three times with DPBS and then permeabilization was conducted with 0.1 % Triton X-100 (11869, Merck Millipore) for 5 min. Cells were blocked with 1 % BSA (160069, MP Biomedicals, Santa Ana, CA, USA) for 30 min. Alexa Flour 568 Phalloidin (A12380, Thermo Fisher Scientific) was used for staining of F-actin. After staining, cell washed three times with PBS-T (0.1% Tween 20 in PBS) and then re-blocked for 30 min in a humidified dark chamber. The cells were labeled with vinculin (MA5-11690, Thermo Fisher Scientific) for 3 h. Alexa Flour 488 anti-mouse secondary antibody (A28175, Thermo Fisher Scientific)

were used. DAPI mounting solution (ab104139, Abcam) was used for staining of nuclei. Confocal imaging analysis was conducted with LSM 800 (ZEISS, Germany). Distance from the nucleus was measured using ImageJ (NIH, Bethesda, MD, USA) and intensity mean value of F-actin and vinculin was analyzed by ZEN 2.3 lite software (ZEISS).

11. Wound healing assay

hTERT RPE-1, #43, and #81 ($3x10^5$ cells/well) were seeded into 6-well plates (3506, Corning) for 1 day and then the monolayer was scratched with a 1 ml pipette tip in a straight line. After the culture medium was replaced with fresh culture medium, it was incubated for 24 h. Cells were observed at 0, 6, 12, and 24 h with an inverted microscope (Eclipse Ts2, Nikon, Japan). Cell size was measured using NIS-Elements software (Nikon, Tokyo, Japan). Wound closure areas were calculated using ImageJ.

12. Fibronectin adhesion assay

Human plasma fibronectin (1 mg/ml) (2549971, Merck Millipore) was diluted with DPBS to 2.5 μg/ml. The diluted plasma fibronectin was dispensed into 96-well plates (50 μl) and incubated for 1 h at room temperature. hTERT RPE-1, #43, and #81 ($3x10^5$ cells/well) were seeded into the designated wells. After incubation for 2 h in a

37° C incubator, the cells were washed with serum-free DMEM: F-12 1:1 (1X) 3 times. Then, they were incubated for 30 min with 200 μl DMEM: F-12 1:1 (1X) supplemented with 10% heat-inactivated FBS in a 37° C incubator. EZ-Cytox solution (10 μl) was added to each well, and the value was measured at 450 nm wavelength after incubation for 2 h.

13. Statistical analysis

The Student's t-test and two-way ANOVA using GraphPad Prism 5 software (GraphPad Software Inc., La Jolla, CA, USA) analyzed the statistical significance of differences between individuals. Error bars represented mean ± SD. (*$p<0.05$, **$p<0.01$, and ***$p<0.001$).

RESULTS

1. The *MYH8* truncated mutation R1292X found in poor prognosis AML patients

MYH8 R1292X mutation was found in 1 of 53 adult AML patient samples using WES and an additional 3 of 156 from the diagnosed adult AML cohort using targeted re-sequencing.

One of the clinical features of patients with *MYH8* R1292X mutation was that all have experienced a recurrence. The Relapse-free survival (RFS) period ranged from 3.8 to 20.9 months and two patients relapsed less than a year. One patient had an additional FLT3-ITD (Internal Tandem Duplication) mutation, which is an important factor in AML prognosis [66,67]. The cytogenetic features of the four patients were normal karyotype in two patients, inv (16)(p13.1q22) in one patient, and trisomy 8 in one patient (Table 2).

Table 2. Clinical information of the patients carrying *MYH8* R1292X

	UPN			
	AML1843	AML733	AML692	AML317
Gender	M	F	M	M
Age at diagnosis	63	60	34	61
FAB classification	M2	M1	M4	M4
Cytogenetics	Normal Karyotype	Trisomy 8	inv(16)(p13.1q22)	Normal Karyotype
Other genetic characteristics	FLT3-ITD	-	-	-
Relapse-free survival (months)	3.8	15.4	8.8	20.9
Overall survival (months)	5.9	NA	60 +	43.2
Status	Dead	NA	Alive	Dead

¶ Abbreviations: UPN, Unique Patient Number; M, Male; F, Female; FLT3, Fms-Like Tyrosine kinase 3; ITD, Internal Tandem Duplication; AML, Acute Myeloid Leukemia; FAB, French-American-British; NA, Not Available

2. *MYH8* R1292X KI cell line established using the CRISPR-Cas9 genome editing system

MYH8 R1292X KI was carried out in hTERT RPE-1, a normal fibroblast cell line, to observe intracellular changes induced by the mutation. We obtained two clones, #43 and #81, and confirmed the KI through deep sequencing (Figure. 1A). The *MYH8* R1292X was a stop-gain mutation that resulted in a truncated form of the myosin tail domain. To confirm the induction of the protein truncation by the mutation, we conducted western blotting. The truncated band (148 kDa) was approximately 1/3 smaller than normal size (223 kDa) observed in clone #43 and #81 (Figure 1B). In quantitative real-time PCR, the relative expression of *MYH8* in both *MYH8* mutant cells was lower than that in control cells (Figure. 1C). This decrease in mRNA appeared to be due to the nonsense-mediated mRNA decay (NMD) that removes the premature mRNA produced by the truncation mutation [68].

A.

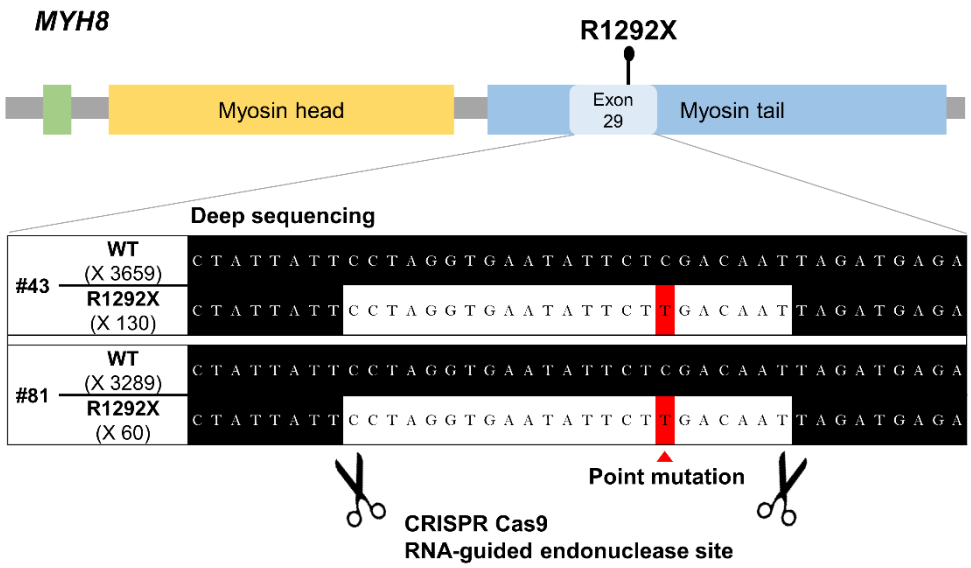
MYH8
R1292X
Myosin head
Exon 29
Myosin tail
Deep sequencing
#43
WT (X 3659)
R1292X (X 130)
#81
WT (X 3289)
R1292X (X 60)
C T A T T A T T C C T A G G T G A A T A T T C T C G A C A A T T A G A T G A G A
C T A T T A T T C C T A G G T G A A T A T T C T T G A C A A T T A G A T G A G A
Point mutation
CRISPR Cas9
RNA-guided endonuclease site

B.

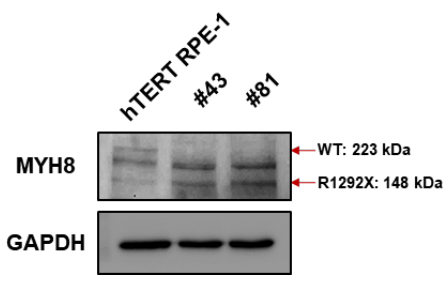
hTERT RPE-1
#43
#81
MYH8
GAPDH
WT: 223 kDa
R1292X: 148 kDa

C.

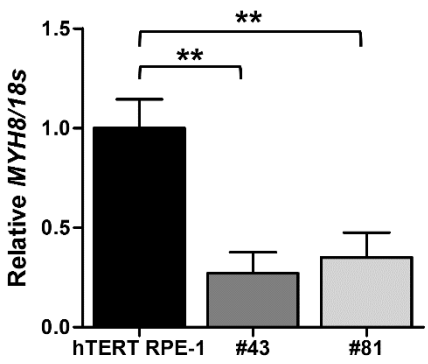
Relative MYH8/18s
1.5
1.0
0.5
0.0
**
**
hTERT RPE-1
#43
#81

Figure 1. Establishment of *MYH8* R1292X cell lines

(A) Schematic representation of *MYH8* R1292X mutation. The *MYH8* R1292X KI clones were obtained using the CRISPR-Cas9 genome editing system. The gene KI was checked through deep sequencing. The white shadow is the RNA-guided endonuclease target site and the red shadow is the point mutation site. (B) MYH8 truncation was confirmed using western blotting. *MYH8* R1292X KI clones #43 and #81 had the truncated form. The molecular weight of wild-type (WT) is 223 kDa (upper band), but #43 and #81 were detected at 148 kDa (lower band). (C) Relatively low expression of *MYH8* was observed in the KI clones through quantitative real-time PCR.

3. *MYH8* R1292X changed the cellular morphology and cell cycle

Since *MYH8* regulates cytoskeleton by binding actin filament [47], we evaluated changes in cell morphology according to the mutation. There was a difference in cell spreading and branches morphology by time-course observation. The cell branches were shorter or almost invisible in mutant cells, whereas control cells had sharp and long elongated on both sides (Figure. 2A). The morphological differences according to the mutation were also confirmed by immunofluorescence staining of F-actin and vinculin. The cell size and spreading area extending from the nucleus was smaller in mutant cells than control cells (Figure. 2B). In addition, mutant cells showed higher expression of F-actin and vinculin, which are related to cell mobility [69-71] at the edge of cells than control cells (Figure. 2C) (marked with white points).

In connection with these characteristics, there was a change in the cell cycle associated with increased cell mobility. The amount of G0/G1 DNA in both mutated cells was lower than control cells. Instead, the DNA contents in the G2/M phase were higher (Figure.

2D). These changes in the cell cycle have been reported to be related to increased cell migration [72,73].

Taken together, the mutation induced the alteration of cell morphology and expression of F-actin and vinculin, and cell cycle which was related to increased cell migration. These results suggested that R1292X mutation affected the regulation of cellular mechanisms involved in *MYH8* functions and cell migration.

A.

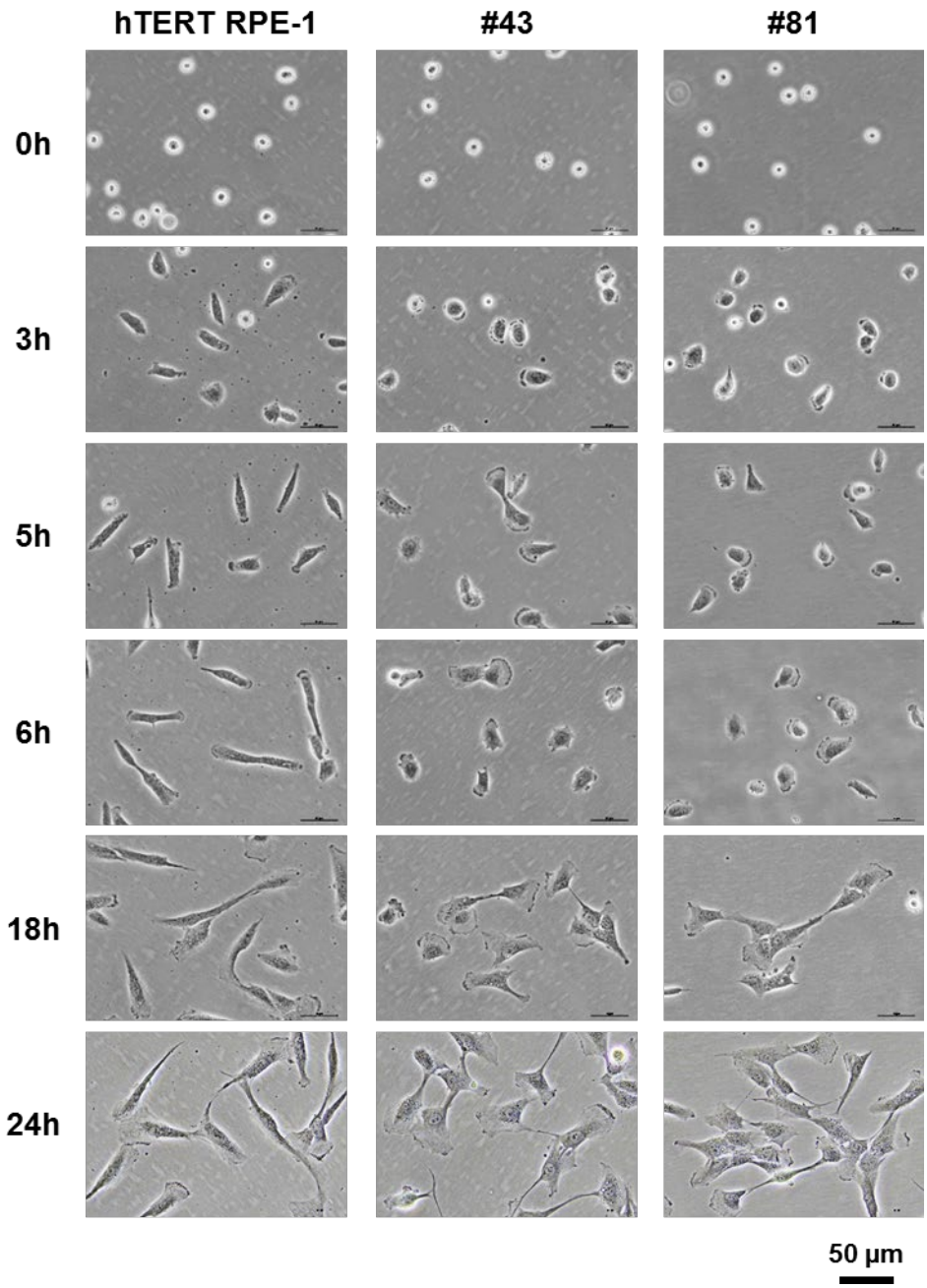

B.

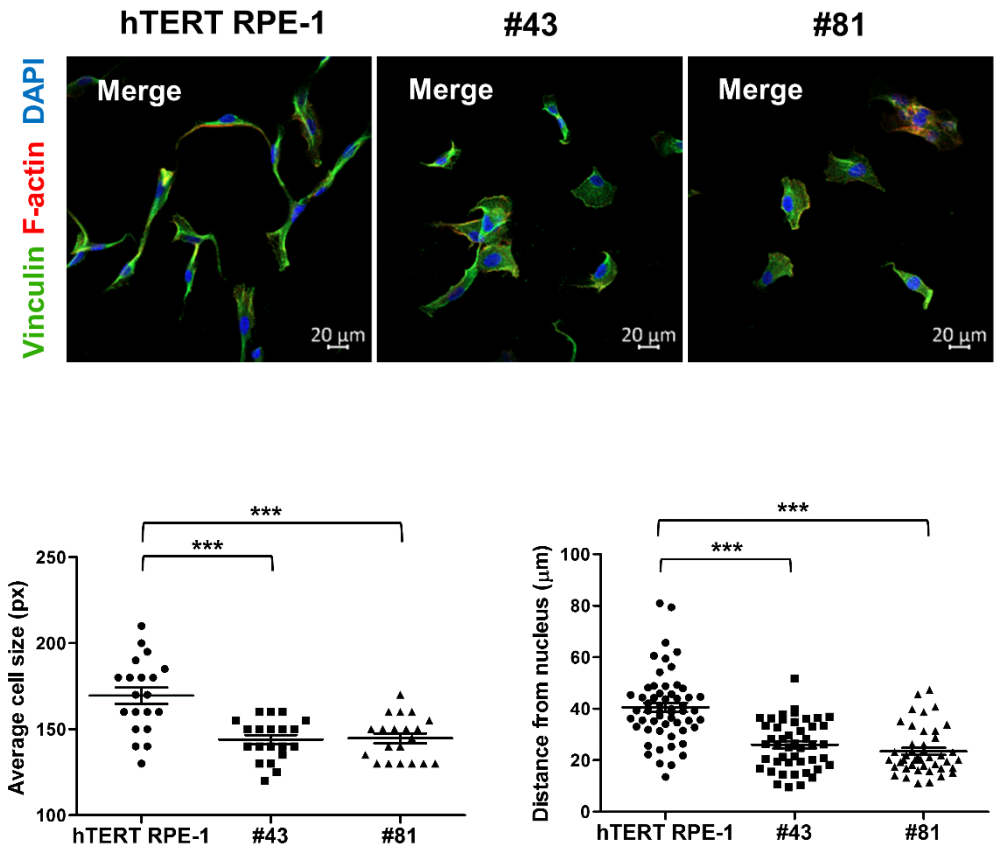
hTERT RPE-1
#43
#81
Vinculin F-actin DAPI
Merge
Merge
Merge
20 μm
20 μm
20 μm
***
***
Average cell size (px)
250
200
150
100
hTERT RPE-1
#43
#81
***
***
Distance from nucleus (μm)
100
80
60
40
20
0
hTERT RPE-1
#43
#81

C.

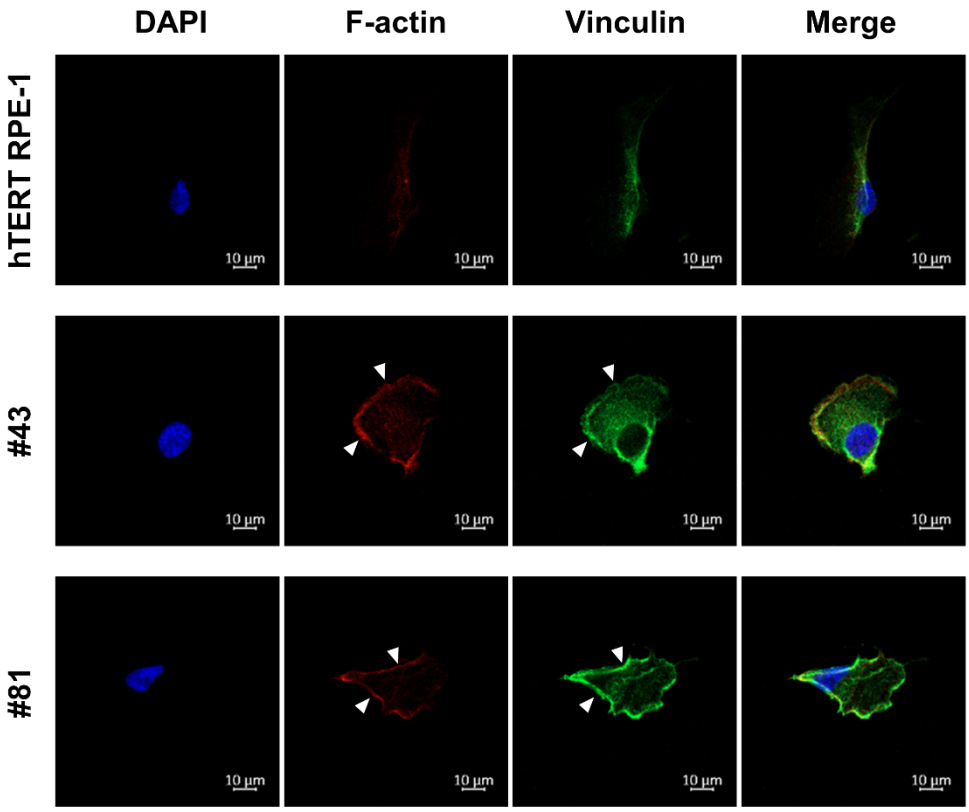
DAPI
F-actin
Vinculin
Merge
hTERT RPE-1
#43
#81
10 μm

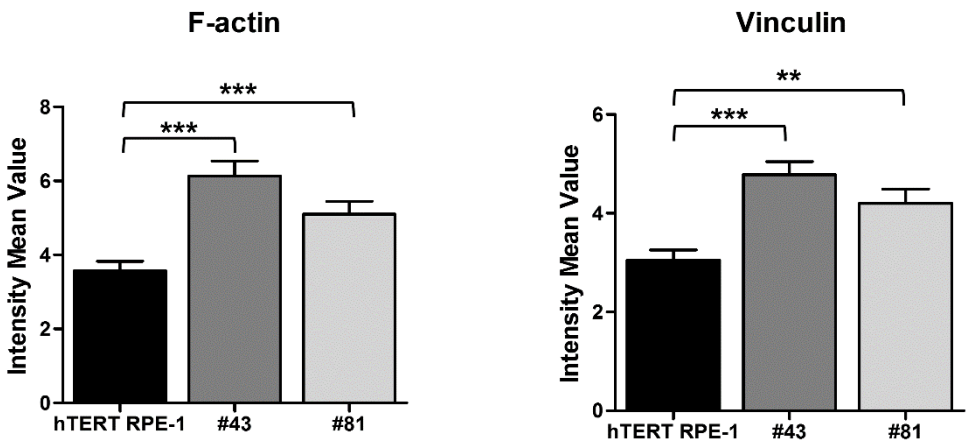
F-actin
Intensity Mean Value
***
***
0
2
4
6
8
hTERT RPE-1
#43
#81
Vinculin
Intensity Mean Value
**
***
0
2
4
6
hTERT RPE-1
#43
#81

D.

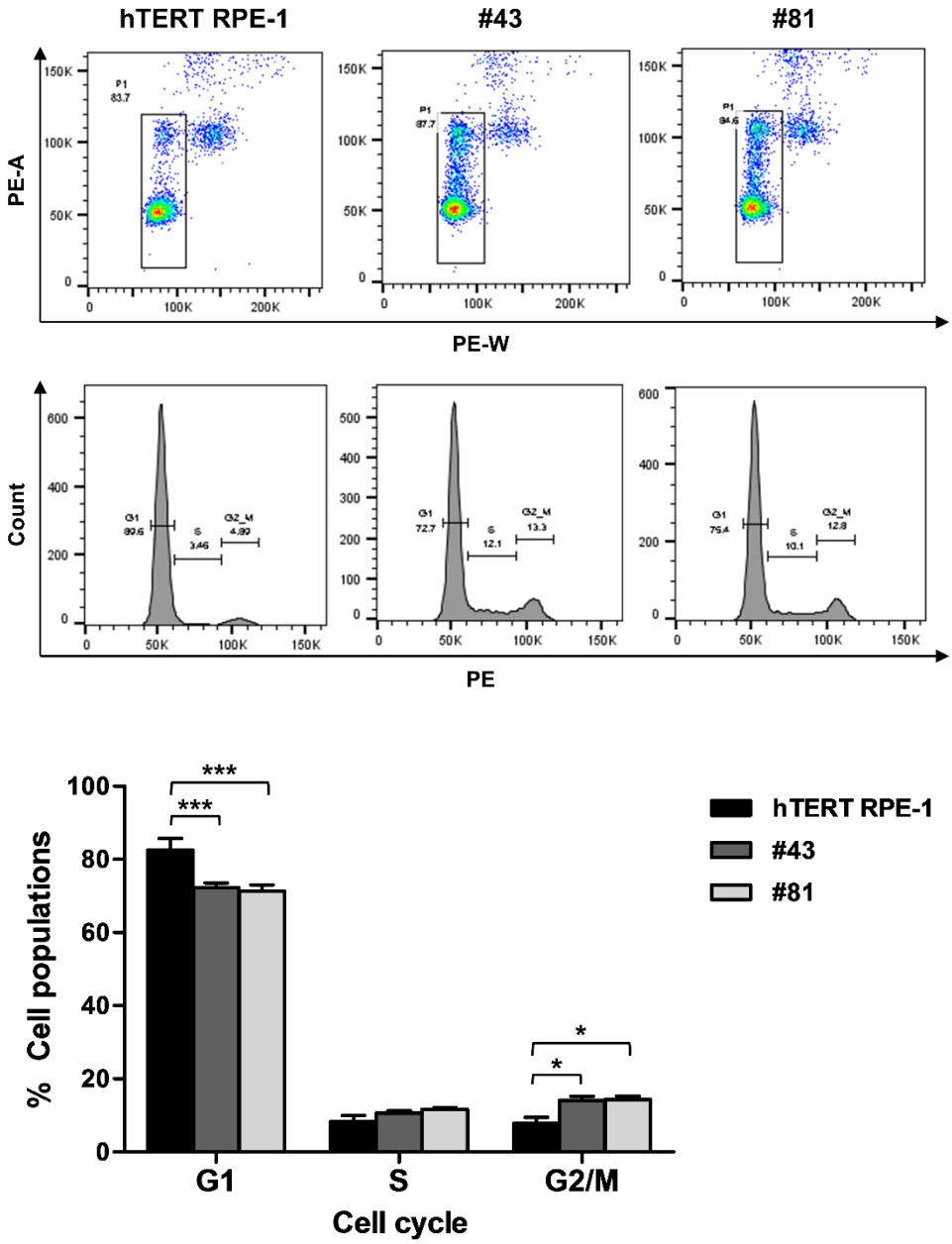
hTERT RPE-1
#43
#81
PE-A
PE-W
Count
PE
% Cell populations
Cell cycle
G1
S
G2/M
hTERT RPE-1
#43
#81
***
***
*
*

Figure 2. Morphology and cell cycle of *MYH8* R1292X cells

(A) Observation of cell morphology by time courses with a bright field microscope. *MYH8* R1292X cells had smaller spreading areas and shorter and less sharp branches than WT. Scale bar: 50 μm. (B) Confocal image of *MYH8* R1292X cells stained with F-actin and vinculin. Scale bar: 20 μm. Cell size was measured using NIS-Elements software. Distance from the nucleus was calculated using ImageJ software. (C) Highly expressed of F-actin and vinculin in cell edges observed in *MYH8* R1292X cells (white points). Scale bar: 10 μm. Intensity mean value was analyzed by ZEN 2.3 lite software. (D) Cell cycle assay of *MYH8* R1292X cells.

4. *MYH8* R1292X induced increase cell migration and EMT-related molecules

Based on the changes in morphological features and cell cycle associated with increased mobility in the mutant cells, we performed wound healing and fibronectin adhesion assays to confirm increased cell migration induced by the mutation.

We identified cell mobility through a wound healing assay to confirm the migration ability increased in *MYH8* mutant cells. Each cell type was seeded with the same number and the monolayer of cells was scratched. Then, wound closure was measured at 0, 6, and 12 h after scratching. We observed that the mutant cell wounds closed earlier than the control cells at 6 h and observed significant differences between the cells at 12 h (Figure. 3A).

The human fibronectin adhesion assay was used to confirm a change in adherence ability. The same numbers of cells were seeded on human fibronectin pre-coated wells, and the number of cells that attached to the fibronectin was measured. Both #43 and #81 cells carrying the *MYH8* mutation had significantly lower adhesion rates than the control cells (Figure. 3B). Together, we confirmed *MYH8*

mutant cells has increased migration ability but reduced adhesion ability.

Increased mobility and decreased adhesiveness are hallmarks of EMT, which observed in a variety of malignant tumors [52]. Western blotting was performed to confirm changes in the EMT markers N-cadherin, Slug, Snail, ZEB1, vimentin and the migration-related molecule phospho-CXCR4 (S339) [74] in *MYH8* mutant cells. EMT regulator molecules were increased and phosphorylation of CXCR4 (S339) was increased in both mutant cells (Figure. 3C).

Taken together, *MYH8* R1292X induced aggressive cancer features of cell migration, upregulation of EMT-related markers and decreased adhesion of cells.

A.

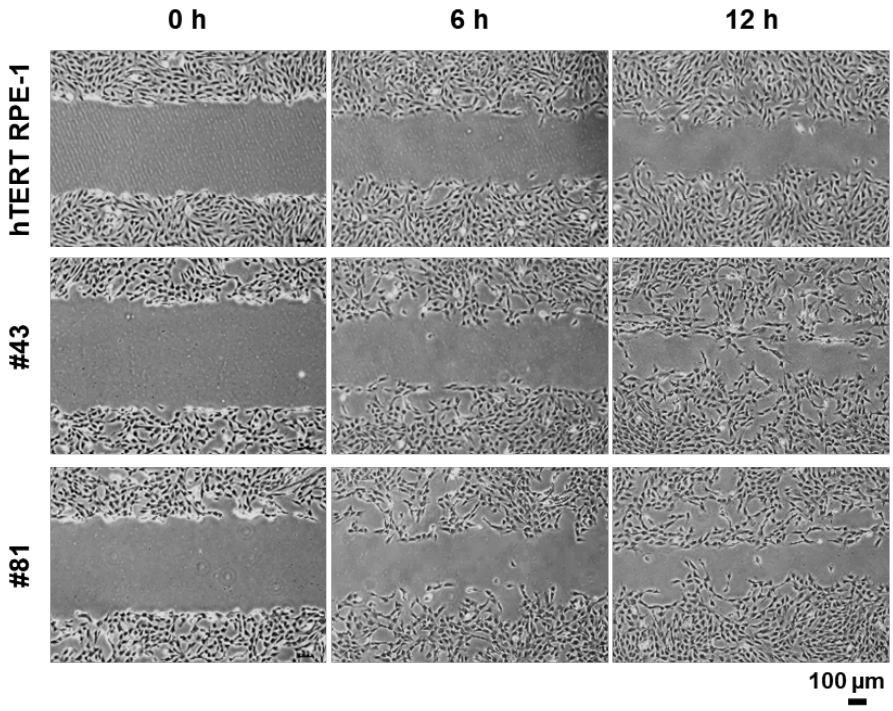
0 h
6 h
12 h
hTERT RPE-1
#43
#81
100 μm

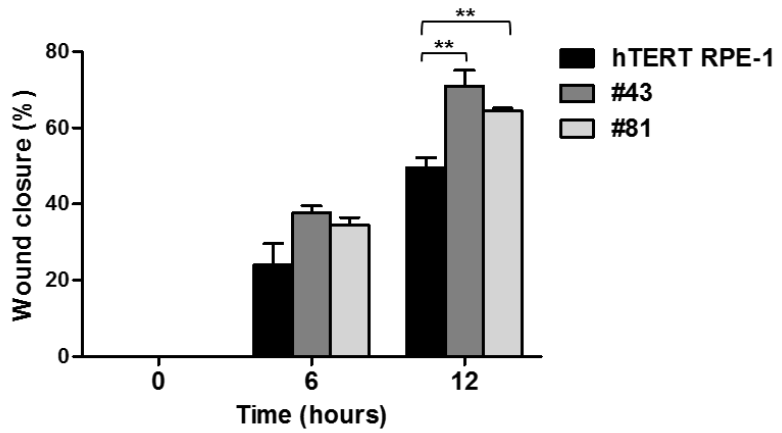
**
**
80
60
40
20
0
Wound closure (%)
0
6
12
Time (hours)
hTERT RPE-1
#43
#81

B.

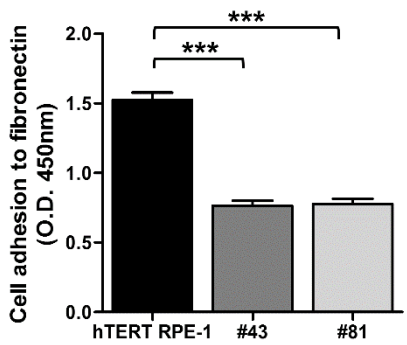

C.

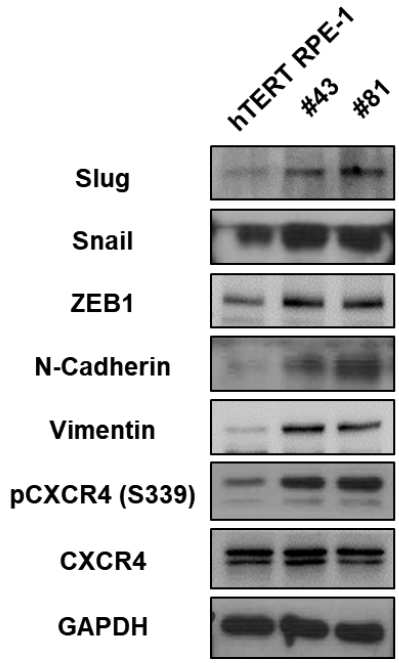

Figure 3. *MYH8* 1292X promoted migration ability and epithelial–mesenchymal transition

(A) A wound healing assay was performed to evaluate cell migration ability. Cells were observed at 0, 6, and 12 h. Wound closure areas were calculated using ImageJ. Scale bar: 100 μm. (B) Cell adhesion ability was evaluated using a human plasma fibronectin adhesion assay. Cells were seeded on human plasma fibronectin coated 96-well plates. After incubation, the number of cells remaining after washing was measured using the OD value. (C) Western blotting of mesenchymal markers, EMT transcriptional markers, and migration marker. GAPDH was used for loading control.

5. MAPK pathway involved in cell migration and EMT-related molecules in *MYH8* R1292X cells

To identify which signaling pathway was associated with the increased cell mobility and EMT features in the mutant cells, we performed western blotting for some major signal transduction molecules.

Phospho-Akt, phospho-STAT3, and phospho-STAT5 had either reduced levels in mutant cells or similar levels to the control cells. On the other hand, the expression of TGF-β and its subcellular signaling molecules c-Raf, B-Raf, and phospho-Erk (1/2) were increased in both mutant cells (Figure. 4A). To confirm whether the activation of MAPK signaling molecules and EMT-related molecules was induced by activated TGF-β, control cells were treated with 5 ng/ml TGF-β for 48 h. After TGF-β treatment, levels of the MAPK signaling molecules c-Raf, B-Raf, and phospho-Erk (1/2) increased, as did levels of EMT TFs Slug, Snail, ZEB1, and of the mesenchymal marker N-cadherin (Figure. 4B).

To confirm whether the increased EMT-related signaling molecule expression was related to the increased MAPK signaling pathway activity, cells were treated with the MAPK signaling

pathway inhibitor trametinib for 48 h and western blotting of the EMT-related molecules was then performed. When treated with trametinib in serial concentrations, the expression of Slug and Snail decreased in both the #43 and #81 cells. In particular, the expression level of Slug decreased even when a low concentration of inhibitor was applied to #43 cells. On the other hand, ZEB1 expression was not changed by the drug treatment in both mutant cells. The level of phospho-CXCR4 (S339), which is involved in the migration of AML cells [74], decreased upon inhibitor treatment, and total CXCR4 expression also decreased (Figure. 4C). Inhibition of the MAPK signaling pathway by trametinib was confirmed by a decrease in the expression of phospho-Erk (1/2).

The wound healing assay was performed after treatment with 3 μM trametinib to determine if the cell mobility was increased due to the elevated EMT factor levels by the activated MAPK signaling pathway. Observation for 24 h revealed that the wound closure area was larger in the mutant than control cells when treated with trametinib. The difference between the cells was most significant at 24 h (Figure. 4D). These data show that migration in the mutant cells is more sensitively regulated by inhibiting the MAPK signaling pathway than in control cells.

Taken together, our data demonstrate that activation of the MAPK pathway by TGF-β is involved in the increased cell migration and induction of EMT molecules occurred by *MYH8* R1292X.

A.

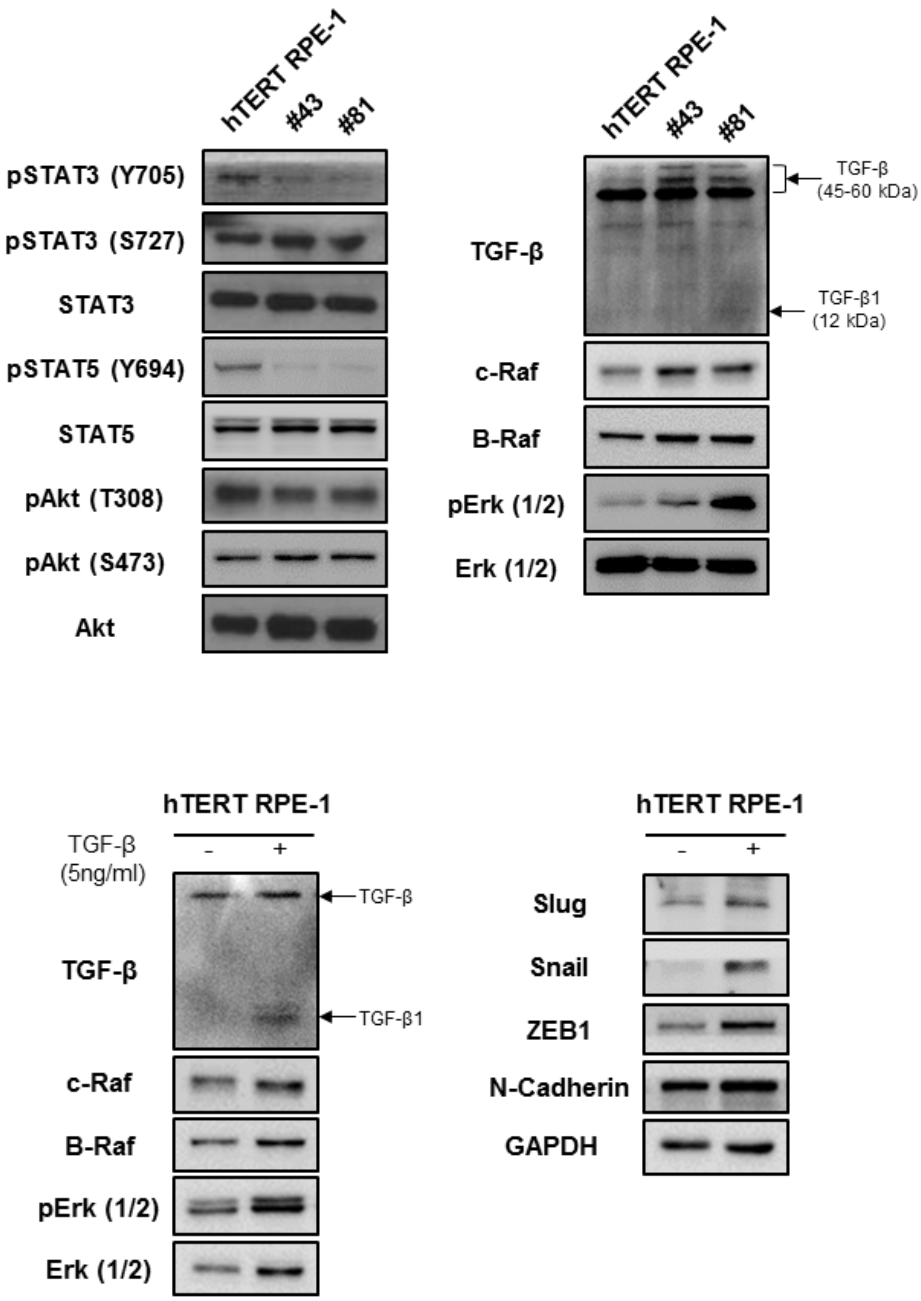
hTERT RPE-1
#43
#81
pSTAT3 (Y705)
pSTAT3 (S727)
STAT3
pSTAT5 (Y694)
STAT5
pAkt (T308)
pAkt (S473)
Akt
hTERT RPE-1
#43
#81
TGF-β
(45-60 kDa)
TGF-β1
(12 kDa)
TGF-β
c-Raf
B-Raf
pErk (1/2)
Erk (1/2)
hTERT RPE-1
TGF-β
(5ng/ml)
-
+
TGF-β
TGF-β1
TGF-β
c-Raf
B-Raf
pErk (1/2)
Erk (1/2)
hTERT RPE-1
-
+
Slug
Snail
ZEB1
N-Cadherin
GAPDH

B.

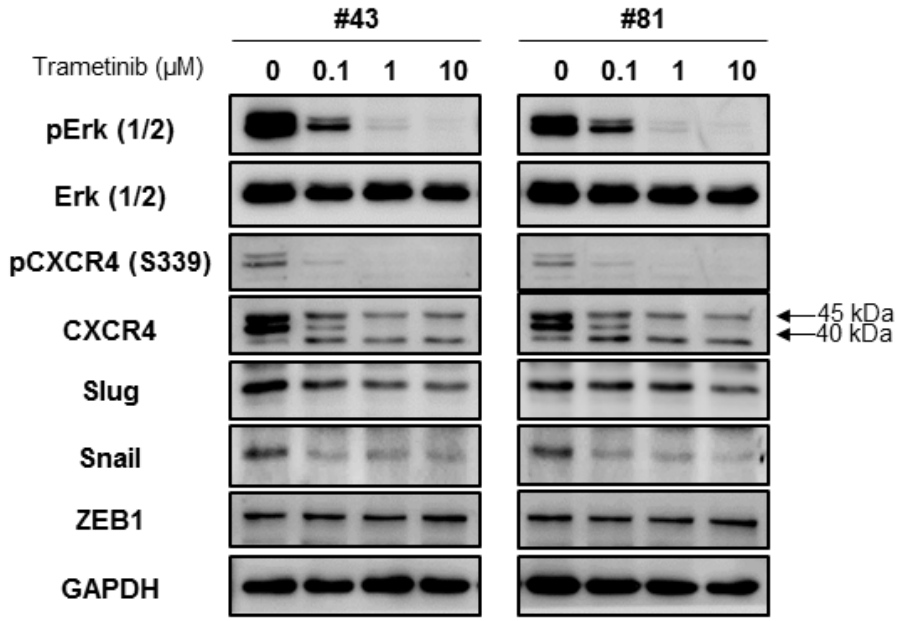
#43
#81
Trametinib (μM)
0 0.1 1 10
0 0.1 1 10
pErk (1/2)
Erk (1/2)
pCXCR4 (S339)
CXCR4
45 kDa
40 kDa
Slug
Snail
ZEB1
GAPDH

C.

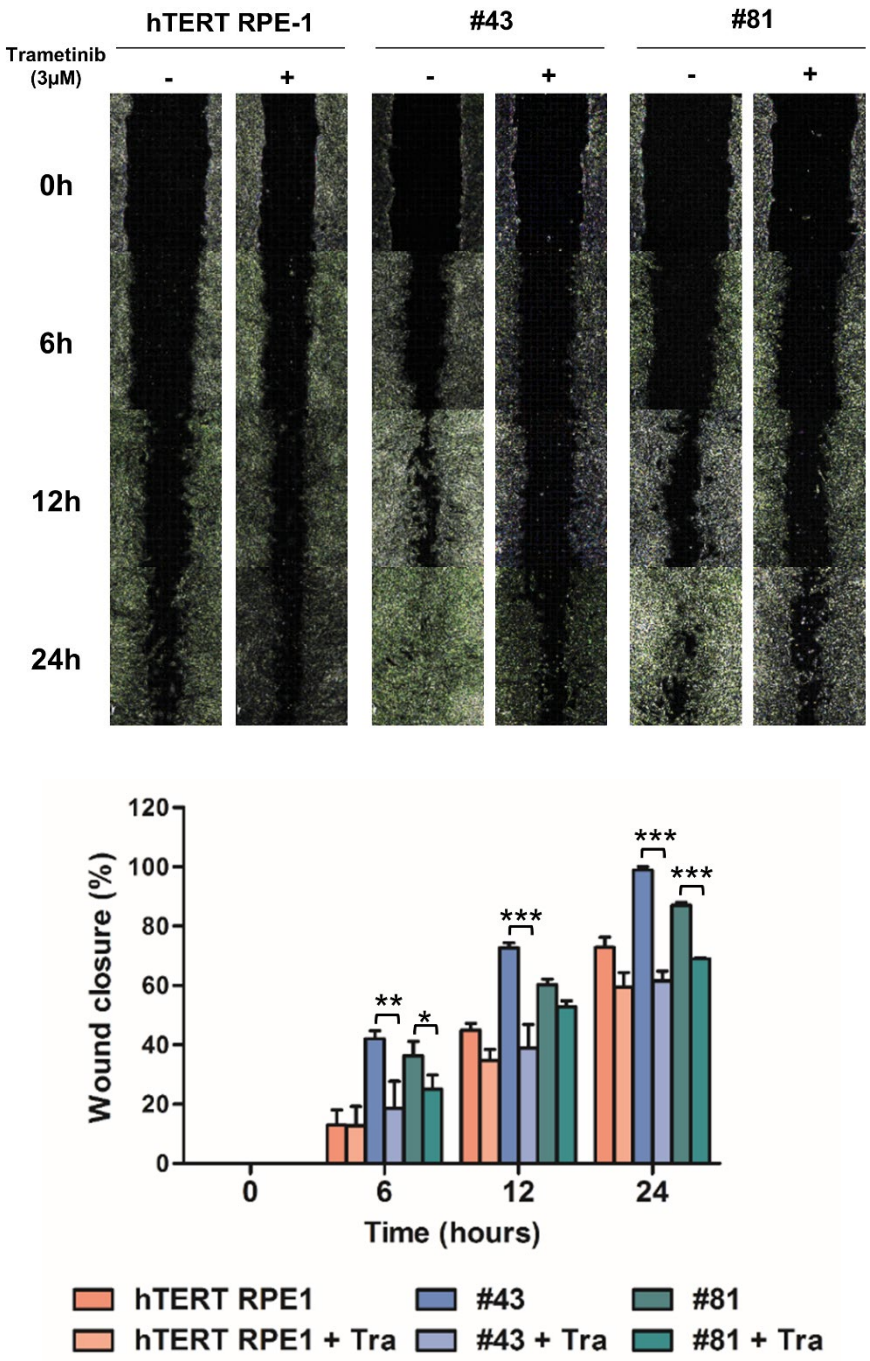
hTERT RPE-1
#43
#81
Trametinib (3μM)
-
+
-
+
-
+
0h
6h
12h
24h
Wound closure (%)
120
100
80
60
40
20
0
**
*
***
***
***
0
6
12
24
Time (hours)
hTERT RPE1
hTERT RPE1 + Tra
#43
#43 + Tra
#81
#81 + Tra

Figure 4. MAPK pathway involved in promoted migration ability and epithelial–mesenchymal transition in *MYH8* R1292X cells

(A) Western blotting confirmed the STATs, Akt, TGF-β, Raf, and Erk levels. Among them, TGF-β, Raf, and Erk were increased in KI clones. (B) hTERT RPE-1 cells were treated with hTGF-β (5 ng/ml) for 48 h to confirm the activation of MAPK and EMT transcription factor (TF) molecules through TGF-β. (C) Confirmation of the regulation of EMT TF molecules and migration marker by the MAPK pathway. Cells were treated with trametinib and then assessed using western blotting. Erk, CXCR4, Slug, and Snail expressions were decreased following treatment of trametinib. (D) The wound healing assay was performed to determine whether the reduction of MAPK and EMT TF by trametinib affected cell movement. Wound closure areas were calculated using ImageJ.

6. Cell proliferation and cell migration-related molecule *MMP13* activated in *MYH8* R1292X cells

Patients with *MYH8* R1292X all had a recurrence, which is a feature of malignant tumors, and activated MAPK signaling pathway is involved in cell proliferation [75]. We, therefore, conducted a proliferation assay to determine whether the mutation conferred proliferative ability.

After seeding the same number of cells, the growth rates from 0 to 3 days were compared among the cells. The growth rate on day three in both #43 and #81 was significantly higher and day two as well, especially for #43, compared to the control cells (Figure. 5A). Another feature of malignant tumors is that they can grow in limited spaces and environments. We seeded each cell types in a 96-well plate with 500, 1,500, and 3,000 cells/well to assess this feature. The growth rate after one week was confirmed by comparing relative OD values. Both mutant cell lines were more proliferative than the control in 1,500- and 3,000-cell seeding conditions, even with limited space and crowded condition (Figure. 5B).

The proliferation assay results demonstrated that the mutant cells showed better proliferation ability than the control cells both in viable environments and even where it was difficult to survive.

To identify the extracellular matrix (ECM) degradation enzymes that play a role in the mobility of *MYH8* R1292X cells, I measured the expression levels of eight MMPs by RT-PCR. When compared to the control cells, only the expression of *MMP13* was increased in both mutant cell lines. *MMP13* expression in mutant cells was approximately 10 fold higher in #43 cells and 25 fold higher in #81 cells (Figure. 5C).

To confirm that the increased *MMP13* levels were also regulated by MAPK signaling, RT-PCR was conducted to assess the expression level of *MMP13* after treatment with 0.1 μM trametinib in #43 and #81 cells. In both mutant cell lines, the expression of *MMP13* decreased after drug treatment (Figure. 5D).

Taken together, *MMP13* was increased in both mutant cells, and its expression was regulated by the MAPK pathway inhibitor that regulates cell migration and EMT molecule expression in mutant cells. Thus, increased *MMP13* may be related to the increased cell migration of *MYH8* R1292X cells.

A.

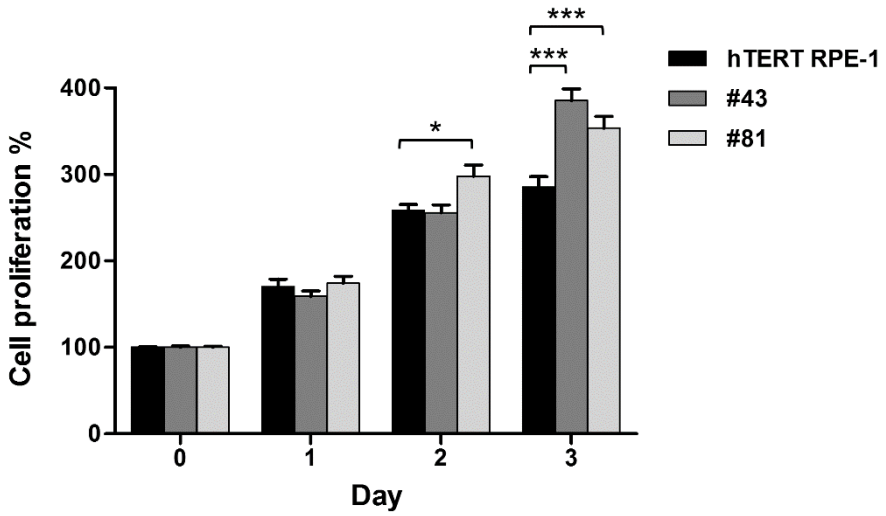
Cell proliferation %
400
300
200
100
0
0
1
2
3
Day
*
***
***
hTERT RPE-1
#43
#81

B.

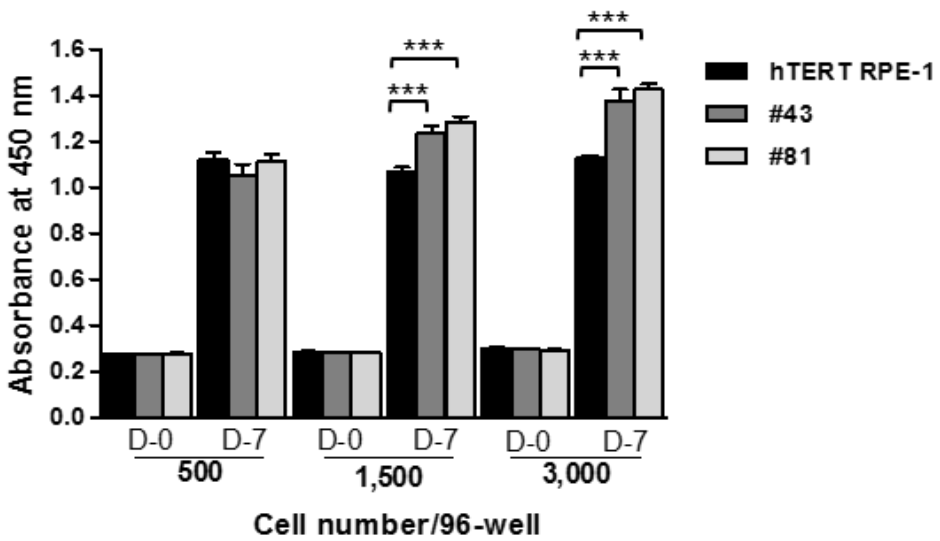
Absorbance at 450 nm
1.6
1.4
1.2
1.0
0.8
0.6
0.4
0.2
0.0
D-0
D-7
500
1,500
3,000
Cell number/96-well
***
***
***
***
hTERT RPE-1
#43
#81

C.

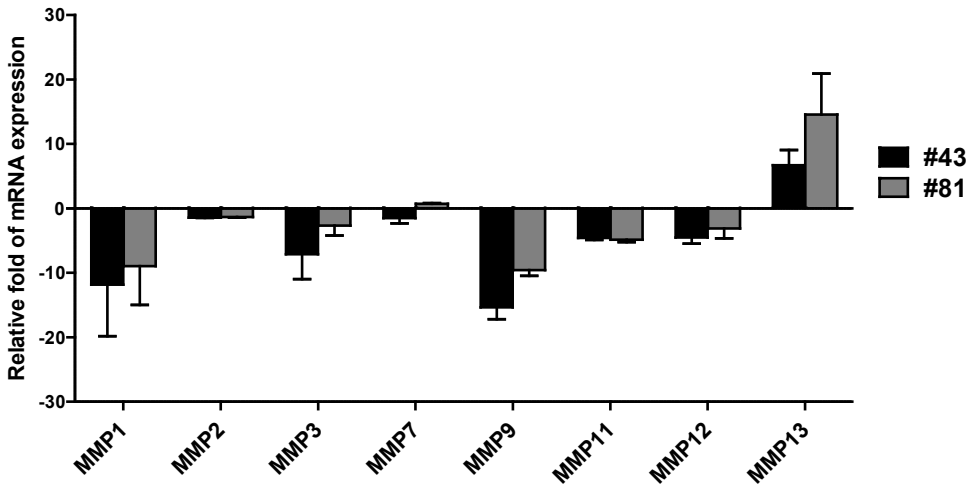
Relative fold of mRNA expression
30
20
10
0
-10
-20
-30
MMP1
MMP2
MMP3
MMP7
MMP9
MMP11
MMP12
MMP13
#43
#81

D.

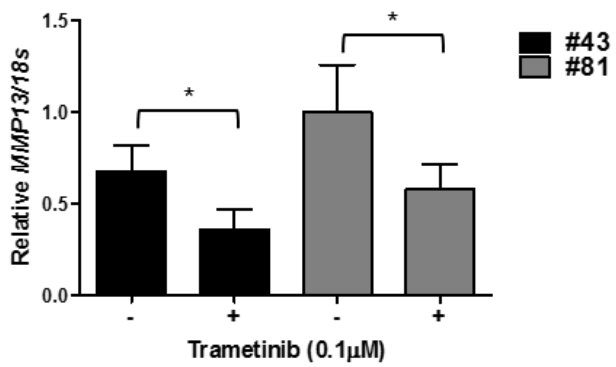
Relative MMP13/18s
1.5
1.0
0.5
0.0
*
*
-
+
-
+
Trametinib (0.1μM)
#43
#81

Figure 5. Increased cell proliferation and upregulation of *MMP13* in *MYH8* R1292X cells

(A) Proliferation assay was used to confirm the difference in growth rate. Growth rates from 0 to 3 days were compared through OD values. (B) To confirm proliferation ability in a limited growing space, 500, 1,500, and 3,000 cells/well were seeded in a 96-well plate. The number of cells after 1 week was confirmed using OD values. (C) Real-time PCR was performed to identify the MMP involved in cell migration in *MYH8* R1292X cells. Of the 8 MMPs, only *MMP13* increased in *MYH8* knock-in (KI) cells compared with the control. (D) After trametinib treatment for 48 h, RT-PCR confirmed the decrease of *MMP13* expression. Gene expression was normalized to 18S rRNA.

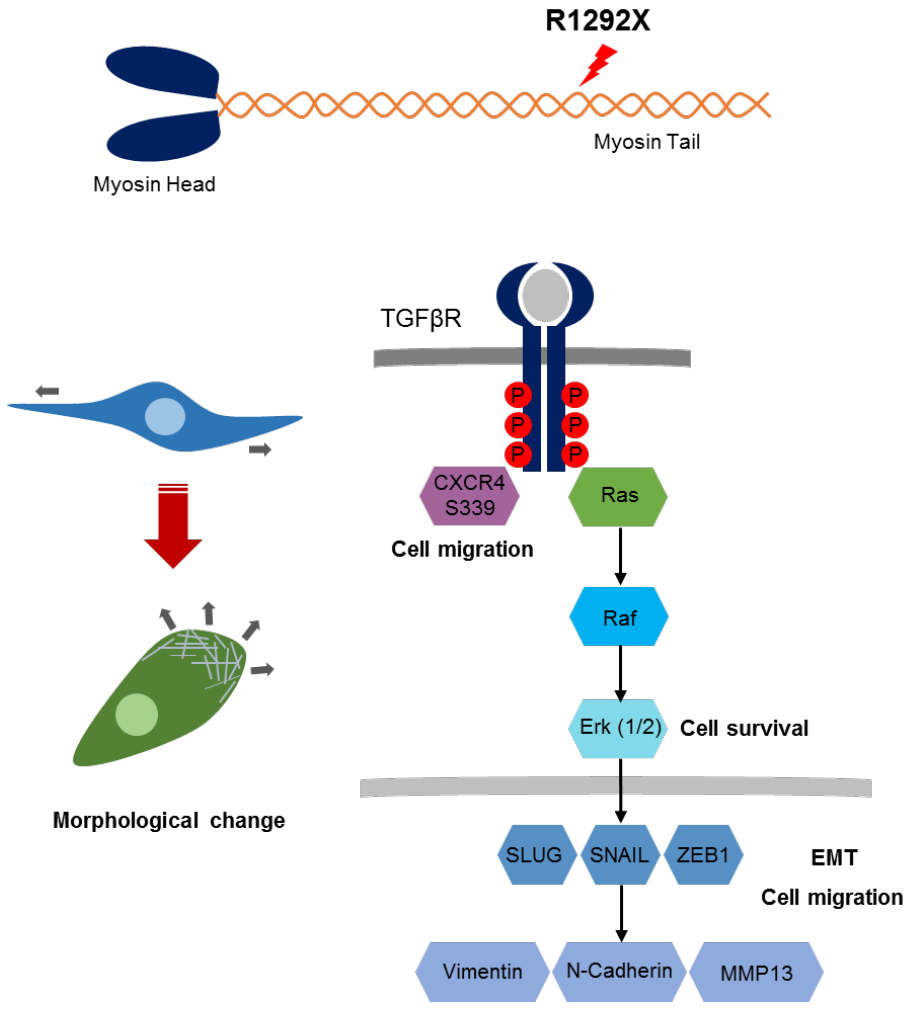

Figure 6. Schematic illustration of *MYH8* R1292X effects on cell

DISCUSSION

MYH8 truncating mutation, which has no previously reported functions in cancer, was found in our AML cohort with poor prognosis. We conducted staining of cell morphology, cell cycle assay, wound healing assay, proliferation assay, and screening of signaling pathways to investigate whether this mutation had a prognostic effect in cancer cells. Our data showed that *MYH8* R1292X might be related to AML progress through by affecting cell migration, proliferation, and EMT molecules through RAS-MAPK signaling (Figure. 6).

We constructed cell lines to identify the characteristics induced by the mutation using CRISPR-Cas9 genome editing on hTERT RPE-1, a normal cell line. We performed knock-in in normal cells instead of tumor cells to explore the intensity of intracellular function of the mutant itself. In mutant cells, the spreading area decreased compared to control cells. As of our result, the loss of the original function of myosin by the genomic alteration was consistent with the well-known fact of myosin involvement in cell spreading [76]. We assumed that the increased mobility of mutant cells was partially related to decreasing the cell's spreading area as known to reduce cell mobility in the increased cell spreading area [77].

We identified upregulated EMT markers as key features of metastasis and drug resistance in a large number of aggressive tumors. In the case of *MYH8* truncated mutation cells, TGF-β was upregulated and the RAS-MAPK signaling pathway was activated. The activity of RAS-MAPK signaling induced by TGF-β and the resultant activity of EMT TFs in this study were consistent with previously reported research [78,79]. The EMT TFs increase in hematologic malignancies significantly effects on the myeloid and lymphoid development, leukemia and lymphoma progression [80], suggesting the EMT markers as prognostic indicators. In addition, deregulation of the RAS-MAPK pathway commonly occurs in hematologic cancers, especially in AML, and aberrant RAS-MAPK signals affect various cellular aspects such as gene transcription, cell cycle, and cell death mechanism. For these reasons, the RAS-MAPK pathway has been proposed to be an attractive therapeutic target in hematologic cancer as well as in solid tumors [81,82].

One of the characteristics of EMT and cell migration is an increased activity of matrix metalloproteinases (MMPs) for ECM degradation. The MMPs are not only essential proteases to degrade components of the ECM, but also regulators in cancer progression by triggering cell proliferation, migration, adhesion, angiogenesis, and apoptosis [83,84]. In particular, MMP-13 (collagenase-3) find to be

overexpressed in a variety of invasive and metastatic cancers including breast cancer, head and neck carcinomas, chondrosarcomas, and skin carcinomas [85], and it also has been shown to affect the survival rate of cancer patients in recent studies [86,87]. Together, the overexpression of *MMP13* might play an important role in the progression of hematological malignancies as in other cancers.

To date, the function of *MYH8* mutations in cancer is not well known and the correlation of myosin in any tumors has been relatively limited. The alteration in *MYH8* was the second most abundant in leukemia following colorectal adenocarcinoma according to the cBioPortal (Figure. 7A). Supporting our data, there are many truncating mutations similar to R1292X, which often occurs in the myosin tail domain (Figure. 7B, C). It can be assumed through this database that the *MYH8* truncating mutation might have impacts on various cancers; however, this has not yet been revealed. It should be noted that even if the mutation did not appear in the locus as a hotspot, the truncating mutation in the myosin tail domain is meaningful as function loss of *MYH8* contribution to carcinogenesis.

In conclusion, our study showed that *MYH8* truncating mutation effects on biological functions in cells including morphological change, increased migration, and expression of EMT TFs. This study is the first to describe the influence of *MYH8* tail truncation mutation in

cells and to examine the possibility of a correlation between *MYH8* mutation and cancer progress.

A.

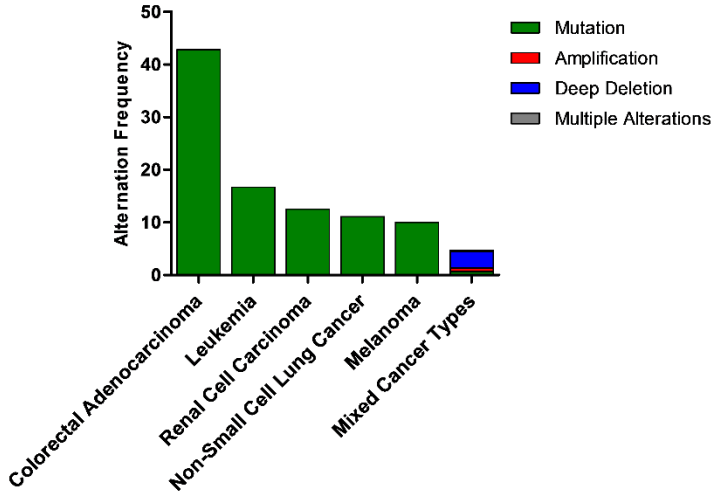
Alternation Frequency
50
40
30
20
10
0
Mutation
Amplification
Deep Deletion
Multiple Alterations
Colorectal Adenocarcinoma
Leukemia
Renal Cell Carcinoma
Non-Small Cell Lung Cancer
Melanoma
Mixed Cancer Types

B.

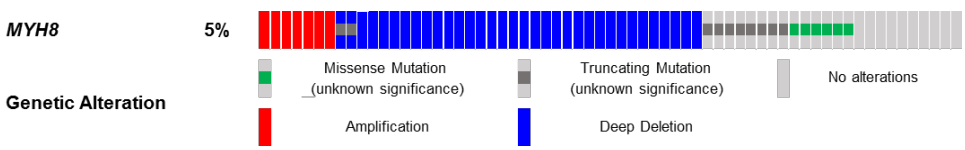
MYH8
5%
Genetic Alteration
Missense Mutation
(unknown significance)
Truncating Mutation
(unknown significance)
No alterations
Amplification
Deep Deletion

C.

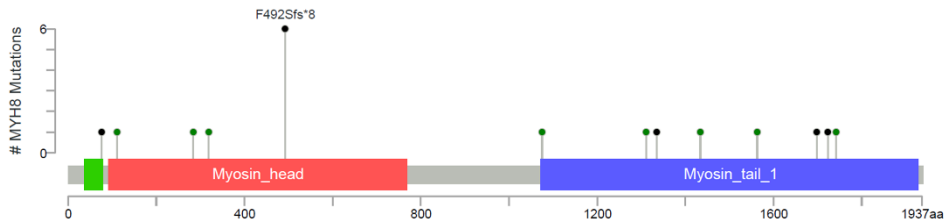
F492Sfs*8
MYH8 Mutations
6
0
Myosin_head
Myosin_tail_1
0
400
800
1200
1600
1937aa

Figure 7. Summary of *MYH8* alterations in various cancers

(A) Cell line genetic data of 1,087 various cases were obtained from the cBioPortal database and analyzed for *MYH8* alterations. The graph shows the type and sequence of cancer with *MYH8* alterations and the types of alteration in that cancer. Leukemia is the second most frequent cancer with *MYH8* alterations following the colorectal adenocarcinoma. (B) The % of *MYH8* alteration and subdivided the types of alterations. (C) Illustration of the locus of the *MYH8* alterations.

REFERENCES

1. Miettinen M, Lasota J. KIT (CD117): a review on expression in normal and neoplastic tissues, and mutations and their clinicopathologic correlation. *Appl Immunohistochem Mol Morphol.* 2005;13(3):205-220.
2. Ayatollahi H, Shajiei A, Sadeghian MH, et al. Prognostic Importance of C-KIT Mutations in Core Binding Factor Acute Myeloid Leukemia: A Systematic Review. *Hematol Oncol Stem Cell Ther.* 2017;10(1):1-7.
3. Ziai JM, Siddon AJ, Education Committee of the Academy of Clinical Laboratory P, Scientists. Pathology Consultation on Gene Mutations in Acute Myeloid Leukemia. *Am J Clin Pathol.* 2015;144(4):539-554.
4. Valent P, Akin C, Sperr WR, et al. Mastocytosis: pathology, genetics, and current options for therapy. *Leuk Lymphoma.* 2005;46(1):35-48.
5. Growney JD, Clark JJ, Adelsperger J, et al. Activation mutations of human c-KIT resistant to imatinib mesylate are sensitive to the tyrosine kinase inhibitor PKC412. *Blood.* 2005;106(2):721-724.
6. Hoermann G, Gleixner KV, Dinu GE, et al. The KIT D816V allele burden predicts survival in patients with mastocytosis and correlates with the WHO type of the disease. *Allergy.* 2014;69(6):810-813.
7. Wakita S, Yamaguchi H, Miyake K, et al. Importance of c-kit mutation detection method sensitivity in prognostic analyses of t(8;21)(q22;q22) acute myeloid leukemia. *Leukemia.* 2011;25(9):1423-1432.
8. Ma Y, Zeng S, Metcalfe DD, et al. The c-KIT mutation causing human mastocytosis is resistant to STI571 and other KIT kinase inhibitors; kinases with enzymatic site mutations show different inhibitor sensitivity profiles than wild-type kinases and those with regulatory-type mutations. *Blood.* 2002;99(5):1741-1744.
9. Chan IJ, Kasprowicz S, Tharp MD. Distinct signalling pathways for mutated KIT(V560G) and KIT(D816V) in mastocytosis. *Clin Exp Dermatol.* 2013;38(5):538-544.
10. Gabillot-Carre M, Lepelletier Y, Humbert M, et al. Rapamycin inhibits growth and survival of D816V-mutated c-kit mast cells. *Blood.* 2006;108(3):1065-1072.
11. Sun J, Pedersen M, Ronnstrand L. The D816V mutation of c-Kit circumvents a requirement for Src family kinases in c-Kit signal transduction. *J Biol Chem.* 2009;284(17):11039-11047.
12. Chian R, Young S, Danilkovitch-Miagkova A, et al. Phosphatidylinositol 3 kinase contributes to the transformation of hematopoietic cells by the D816V c-Kit mutant. *Blood.* 2001;98(5):1365-1373.
13. Chaix A, Lopez S, Voisset E, Gros L, Dubreuil P, De Sepulveda P. Mechanisms of STAT protein activation by oncogenic KIT mutants in

neoplastic mast cells. *J Biol Chem.* 2011;286(8):5956-5966.
14. Swords R, Kelly K, Carew J, et al. The Pim kinases: new targets for drug development. *Curr Drug Targets.* 2011;12(14):2059-2066.
15. Aziz AUR, Farid S, Qin K, Wang H, Liu B. PIM Kinases and Their Relevance to the PI3K/AKT/mTOR Pathway in the Regulation of Ovarian Cancer. *Biomolecules.* 2018;8(1).
16. Mondello P, Cuzzocrea S, Mian M. Pim kinases in hematological malignancies: where are we now and where are we going? *J Hematol Oncol.* 2014;7:95.
17. Zhang X, Song M, Kundu JK, Lee MH, Liu ZZ. PIM Kinase as an Executional Target in Cancer. *J Cancer Prev.* 2018;23(3):109-116.
18. An N, Cen B, Cai H, Song JH, Kraft A, Kang Y. Pim1 kinase regulates c-Kit gene translation. *Exp Hematol Oncol.* 2016;5:31.
19. Omori I, Yamaguchi H, Miyake K, Miyake N, Kitano T, Inokuchi K. D816V mutation in the KIT gene activation loop has greater cell-proliferative and anti-apoptotic ability than N822K mutation in core-binding factor acute myeloid leukemia. *Exp Hematol.* 2017;52:56-64 e54.
20. Warfel NA, Kraft AS. PIM kinase (and Akt) biology and signaling in tumors. *Pharmacol Ther.* 2015;151:41-49.
21. Jin B, Ding K, Pan J. Ponatinib induces apoptosis in imatinib-resistant human mast cells by dephosphorylating mutant D816V KIT and silencing beta-catenin signaling. *Mol Cancer Ther.* 2014;13(5):1217-1230.
22. Jin Y, Lu Z, Cao K, et al. The antitumor activity of homoharringtonine against human mast cells harboring the KIT D816V mutation. *Mol Cancer Ther.* 2010;9(1):211-223.
23. Pan J, Quintas-Cardama A, Kantarjian HM, et al. EXEL-0862, a novel tyrosine kinase inhibitor, induces apoptosis in vitro and ex vivo in human mast cells expressing the KIT D816V mutation. *Blood.* 2007;109(1):315-322.
24. Shah NP, Lee FY, Luo R, Jiang Y, Donker M, Akin C. Dasatinib (BMS-354825) inhibits KITD816V, an imatinib-resistant activating mutation that triggers neoplastic growth in most patients with systemic mastocytosis. *Blood.* 2006;108(1):286-291.
25. Evans E, Gardino A, Hodous B, et al. Blu-285, a Potent and Selective Inhibitor for Hematologic Malignancies with KIT Exon 17 Mutations. *Blood.* 2015;126(23).
26. Evans EK, Hodous BL, Gardino AK, et al. BLU-285, the first selective inhibitor of PDGFR alpha D842V and KIT Exon 17 mutants. *Cancer Res.* 2015;75.
27. Wichmann C, Quagliano-Lo Coco I, Yildiz O, et al. Activating c-KIT mutations confer oncogenic cooperativity and rescue RUNX1/ETO-induced DNA damage and apoptosis in human primary CD34+ hematopoietic progenitors. *Leukemia.* 2015;29(2):279-289.
28. Quail DF, Joyce JA. Microenvironmental regulation of tumor progression and metastasis. *Nat Med.* 2013;19(11):1423-1437.
29. Petrova V, Annicchiarico-Petruzzelli M, Melino G, Amelio I. The

hypoxic tumour microenvironment. *Oncogenesis.* 2018;7(1):10.
30. Yan B, Zemskova M, Holder S, et al. The PIM-2 kinase phosphorylates BAD on serine 112 and reverses BAD-induced cell death. *J Biol Chem.* 2003;278(46):45358-45367.
31. Levy D, Davidovich A, Zirkin S, et al. Activation of cell cycle arrest and apoptosis by the proto-oncogene Pim-2. *PLoS One.* 2012;7(4):e34736.
32. Grundler R, Brault L, Gasser C, et al. Dissection of PIM serine/threonine kinases in FLT3-ITD-induced leukemogenesis reveals PIM1 as regulator of CXCL12-CXCR4-mediated homing and migration. *J Exp Med.* 2009;206(9):1957-1970.
33. Brault L, Menter T, Obermann EC, et al. PIM kinases are progression markers and emerging therapeutic targets in diffuse large B-cell lymphoma. *Br J Cancer.* 2012;107(3):491-500.
34. Teodosio C, Garcia-Montero AC, Jara-Acevedo M, et al. Gene expression profile of highly purified bone marrow mast cells in systemic mastocytosis. *J Allergy Clin Immunol.* 2013;131(4):1213-1224, 1224 e1211-1214.
35. Keeton EK, McEachern K, Dillman KS, et al. AZD1208, a potent and selective pan-Pim kinase inhibitor, demonstrates efficacy in preclinical models of acute myeloid leukemia. *Blood.* 2014;123(6):905-913.
36. Corda G, Sala A. Non-canonical WNT/PCP signalling in cancer: Fzd6 takes centre stage. *Oncogenesis.* 2017;6(7):e364.
37. Raman R, Kotapalli V, Adduri R, et al. Evidence for possible non-canonical pathway(s) driven early-onset colorectal cancer in India. *Mol Carcinog.* 2014;53 Suppl 1:E181-186.
38. Papaemmanuil E, Gerstung M, Bullinger L, et al. Genomic Classification and Prognosis in Acute Myeloid Leukemia. *N Engl J Med.* 2016;374(23):2209-2221.
39. Grimwade D, Ivey A, Huntly BJ. Molecular landscape of acute myeloid leukemia in younger adults and its clinical relevance. *Blood.* 2016;127(1):29-41.
40. Ouderkirk JL, Krendel M. Non-muscle myosins in tumor progression, cancer cell invasion, and metastasis. *Cytoskeleton (Hoboken).* 2014;71(8):447-463.
41. Mazzolini R, Dopeso H, Mateo-Lozano S, et al. Brush border myosin Ia has tumor suppressor activity in the intestine. *Proc Natl Acad Sci U S A.* 2012;109(5):1530-1535.
42. Mazzolini R, Rodrigues P, Bazzocco S, et al. Brush border myosin Ia inactivation in gastric but not endometrial tumors. *Int J Cancer.* 2013;132(8):1790-1799.
43. Schramek D, Sendoel A, Segal JP, et al. Direct in vivo RNAi screen unveils myosin IIa as a tumor suppressor of squamous cell carcinomas. *Science.* 2014;343(6168):309-313.
44. Dunn TA, Chen S, Faith DA, et al. A novel role of myosin VI in human prostate cancer. *Am J Pathol.* 2006;169(5):1843-1854.
45. Yoshida H, Cheng W, Hung J, et al. Lessons from border cell migration

in the Drosophila ovary: A role for myosin VI in dissemination of human ovarian cancer. *Proc Natl Acad Sci U S A.* 2004;101(21):8144-8149.
46. Cao R, Chen J, Zhang X, et al. Elevated expression of myosin X in tumours contributes to breast cancer aggressiveness and metastasis. *Br J Cancer.* 2014;111(3):539-550.
47. Wells L, Edwards KA, Bernstein SI. Myosin heavy chain isoforms regulate muscle function but not myofibril assembly. *EMBO J.* 1996;15(17):4454-4459.
48. Vicente-Manzanares M, Ma X, Adelstein RS, Horwitz AR. Non-muscle myosin II takes centre stage in cell adhesion and migration. *Nat Rev Mol Cell Biol.* 2009;10(11):778-790.
49. Schiaffino S, Rossi AC, Smerdu V, Leinwand LA, Reggiani C. Developmental myosins: expression patterns and functional significance. *Skelet Muscle.* 2015;5:22.
50. Whalen RG, Butler-Browne GS, Gros F. Identification of a novel form of myosin light chain present in embryonic muscle tissue and cultured muscle cells. *J Mol Biol.* 1978;126(3):415-431.
51. Toydemir RM, Chen H, Proud VK, et al. Trismus-pseudocamptodactyly syndrome is caused by recurrent mutation of MYH8. *Am J Med Genet A.* 2006;140(22):2387-2393.
52. Heerboth S, Housman G, Leary M, et al. EMT and tumor metastasis. *Clin Transl Med.* 2015;4:6.
53. Singh A, Settleman J. EMT, cancer stem cells and drug resistance: an emerging axis of evil in the war on cancer. *Oncogene.* 2010;29(34):4741-4751.
54. Shibue T, Weinberg RA. EMT, CSCs, and drug resistance: the mechanistic link and clinical implications. *Nat Rev Clin Oncol.* 2017;14(10):611-629.
55. Li H, Mar BG, Zhang H, et al. The EMT regulator ZEB2 is a novel dependency of human and murine acute myeloid leukemia. *Blood.* 2017;129(4):497-508.
56. Kahlert UD, Joseph JV, Kruyt FAE. EMT- and MET-related processes in nonepithelial tumors: importance for disease progression, prognosis, and therapeutic opportunities. *Mol Oncol.* 2017;11(7):860-877.
57. Chou YS, Yang MH. Epithelial-mesenchymal transition-related factors in solid tumor and hematological malignancy. *J Chin Med Assoc.* 2015;78(8):438-445.
58. Xu J, Lamouille S, Derynck R. TGF-beta-induced epithelial to mesenchymal transition. *Cell Res.* 2009;19(2):156-172.
59. Wendt MK, Allington TM, Schiemann WP. Mechanisms of the epithelial-mesenchymal transition by TGF-beta. *Future Oncol.* 2009;5(8):1145-1168.
60. Katsuno Y, Lamouille S, Derynck R. TGF-beta signaling and epithelial-mesenchymal transition in cancer progression. *Curr Opin Oncol.* 2013;25(1):76-84.
61. Xu W, Yang Z, Lu N. A new role for the PI3K/Akt signaling pathway in

the epithelial-mesenchymal transition. *Cell Adh Migr.* 2015;9(4):317-324.
62. Larue L, Bellacosa A. Epithelial-mesenchymal transition in development and cancer: role of phosphatidylinositol 3' kinase/AKT pathways. *Oncogene.* 2005;24(50):7443-7454.
63. Thomas SJ, Snowden JA, Zeidler MP, Danson SJ. The role of JAK/STAT signalling in the pathogenesis, prognosis and treatment of solid tumours. *Br J Cancer.* 2015;113(3):365-371.
64. Chapnick DA, Warner L, Bernet J, Rao T, Liu X. Partners in crime: the TGFbeta and MAPK pathways in cancer progression. *Cell Biosci.* 2011;1:42.
65. Cho Y, Lee S, Hong JH, et al. Development of the variant calling algorithm, ADIScan, and its use to estimate discordant sequences between monozygotic twins. *Nucleic Acids Res.* 2018;46(15):e92.
66. Kindler T, Lipka DB, Fischer T. FLT3 as a therapeutic target in AML: still challenging after all these years. *Blood.* 2010;116(24):5089-5102.
67. Nakao M, Yokota S, Iwai T, et al. Internal tandem duplication of the flt3 gene found in acute myeloid leukemia. *Leukemia.* 1996;10(12):1911-1918.
68. Jia P, Zhao Z. Impacts of somatic mutations on gene expression: an association perspective. *Brief Bioinform.* 2017;18(3):413-425.
69. Jannie KM, Ellerbroek SM, Zhou DW, et al. Vinculin-dependent actin bundling regulates cell migration and traction forces. *Biochem J.* 2015;465(3):383-393.
70. Rothenberg KE, Scott DW, Christoforou N, Hoffman BD. Vinculin Force-Sensitive Dynamics at Focal Adhesions Enable Effective Directed Cell Migration. *Biophys J.* 2018;114(7):1680-1694.
71. Gardel ML, Schneider IC, Aratyn-Schaus Y, Waterman CM. Mechanical integration of actin and adhesion dynamics in cell migration. *Annu Rev Cell Dev Biol.* 2010;26:315-333.
72. Chu TLH, Connell M, Zhou L, et al. Cell Cycle-Dependent Tumor Engraftment and Migration Are Enabled by Aurora-A. *Mol Cancer Res.* 2018;16(1):16-31.
73. Wang SJ, Wang PZ, Gale RP, et al. Cysteine and glycine-rich protein 2 (CSRP2) transcript levels correlate with leukemia relapse and leukemia-free survival in adults with B-cell acute lymphoblastic leukemia and normal cytogenetics. *Oncotarget.* 2017;8(22):35984-36000.
74. Brault L, Rovo A, Decker S, Dierks C, Tzankov A, Schwaller J. CXCR4-SERINE339 regulates cellular adhesion, retention and mobilization, and is a marker for poor prognosis in acute myeloid leukemia. *Leukemia.* 2014;28(3):566-576.
75. Sun Y, Liu WZ, Liu T, Feng X, Yang N, Zhou HF. Signaling pathway of MAPK/ERK in cell proliferation, differentiation, migration, senescence and apoptosis. *J Recept Signal Transduct Res.* 2015;35(6):600-604.
76. Cramer LP, Mitchison TJ. Myosin is involved in postmitotic cell spreading. *J Cell Biol.* 1995;131(1):179-189.
77. Makowska KA, Hughes RE, White KJ, Wells CM, Peckham M. Specific

Myosins Control Actin Organization, Cell Morphology, and Migration in Prostate Cancer Cells. *Cell Rep.* 2015;13(10):2118-2125.
78. Gui T, Sun Y, Shimokado A, Muragaki Y. The Roles of Mitogen-Activated Protein Kinase Pathways in TGF-beta-Induced Epithelial-Mesenchymal Transition. *J Signal Transduct.* 2012;2012:289243.
79. Zhang YE. Non-Smad pathways in TGF-beta signaling. *Cell Res.* 2009;19(1):128-139.
80. Chen SC, Liao TT, Yang MH. Emerging roles of epithelial-mesenchymal transition in hematological malignancies. *J Biomed Sci.* 2018;25(1):37.
81. Platanias LC. Map kinase signaling pathways and hematologic malignancies. *Blood.* 2003;101(12):4667-4679.
82. Pasmant E, Vidaud D, Ballerini P. RAS MAPK inhibitors deregulation in leukemia. *Oncoscience.* 2015;2(12):930-931.
83. Kudo Y, Iizuka S, Yoshida M, et al. Matrix metalloproteinase-13 (MMP-13) directly and indirectly promotes tumor angiogenesis. *J Biol Chem.* 2012;287(46):38716-38728.
84. Gialeli C, Theocharis AD, Karamanos NK. Roles of matrix metalloproteinases in cancer progression and their pharmacological targeting. *FEBS J.* 2011;278(1):16-27.
85. Pendas AM, Uria JA, Jimenez MG, Balbin M, Freije JP, Lopez-Otin C. An overview of collagenase-3 expression in malignant tumors and analysis of its potential value as a target in antitumor therapies. *Clin Chim Acta.* 2000;291(2):137-155.
86. Chang HJ, Yang MJ, Yang YH, Hou MF, Hsueh EJ, Lin SR. MMP13 is potentially a new tumor marker for breast cancer diagnosis. *Oncol Rep.* 2009;22(5):1119-1127.
87. Zhang B, Cao X, Liu Y, et al. Tumor-derived matrix metalloproteinase-13 (MMP-13) correlates with poor prognoses of invasive breast cancer. *BMC Cancer.* 2008;8:83.

국문 초록

급성골수성백혈병은 골수계줄기세포 및 골수아세포와 같은 미분화 세포에 돌연변이 등의 문제가 생겨 미성숙 백혈구 세포가 골수 내에 비정상적으로 증식하면서 정상적인 혈액 세포의 기능과 생성을 저해하는 암이다. 급성골수성백혈병은 혈액암 중에서도 발생률 대비 사망률이 높으며 5년 상대생존율이 가장 낮은 것으로 알려져 있다. 대다수 환자들은 화학요법에 대해 좋은 반응성을 보이나 높은 재발률이 치료의 한계로 알려져 있다. 최근 발전된 차세대 염기서열 분석을 통해 *FLT3*, *NPM1*, *DMNT3A*, *IDH1/2*의 돌연변이가 급성골수성백혈병의 주요 돌연변이로 밝혀졌지만 암세포의 높은 이질성으로 인해 치료율은 여전히 부족한 상태이다. 따라서, 치료율 향상을 위한 돌연변이에 대한 다각적인 분자 생물학적 연구와 새로운 표적 발굴이 필요한 상태이다.

본 연구에서는 기존에 밝혀진 돌연변이인 중심부결합인자 급성골수성백혈병과 비만세포 신생물에서 높은 비율로 발생하면서 불량한 예후를 야기하는 1) *KIT* D816V 대한 기존에 보고되지 않았던 새로운 측면의 분자생물학적 연구와 2) 새롭게 발굴한 *MYH8* R1292X의 세포 내 기능 분석 연구를 진행하였다.

1) *KIT* D816V 돌연변이는 중심부결합인자 급성골수성백혈병에서 30% 가량 발생하며 약물에 대한 저항성과 불량한 예후를 야기한다. D816V에 대한 다양한 분자생물학적 연구가 진행되고 있지만 치료율 향

상을 위한 연구는 여전히 필요한 상태이다. 본 연구에서 *KIT* D816V 돌연변이 여부에 따라 변화하는 주요 신호 분자들의 스크리닝을 통해 돌연변이 세포에서 핌 키나아제 1, 2, 3 가 모두 증가 되어 있음을 확인하였다. 본 연구에서는 증가된 핌 키나아제가 돌연변이 세포의 증식과 생존 그리고 약물 반응성에 관여하는 것을 밝혔으며 재발과 관계되어 있는 세포의 이동성에도 관여함을 확인하였다. *KIT* D816V 돌연변이 세포는 약 2배 이상 높은 세포 이동능을 가지며 이러한 이동성은 핌 키나아제 조절을 통해 저하됨을 확인하였다. 더 나아가, 크리스퍼 유전자 가위를 통해 동일한 티로신 키나아제 도메인에 발생하는 *KIT* N822K 를 야생형으로 치환하여 분자신호를 비교분석한 결과 증가된 핌 키나아제는 *KIT* D816V 세포의 특이적 특징임을 확인하였다. 본 연구결과를 종합하면 증가된 핌 카나아제는 *KIT* D816V 세포에서 중요한 분자생물학적 역할을 하며 따라서 이를 새로운 치료적 표적으로 제시한다.

2) 새로운 급성골수성백혈병의 예후적/치료적 표적을 발굴하기 위해 209개 시료에서 전장엑솜시퀀싱과 표적시퀀싱을 수행하였고 이를 통해 *MYH8* 절단돌연변이인 R1292X 를 발굴하였다. 이 돌연변이를 가지는 4명의 환자들은 모두 재발을 경험한 특징이 있었고 현재까지 *MYH8* 돌연변이와 암과의 상관관계는 보고되지 않았다. 따라서, 본 연구에서는 세포에서의 *MYH8* R1292X 의 기능을 분석하여 급성골수성백혈병 진행에 미칠수 있는 영향을 탐색하였다. 기능 분석을 위해 크리스퍼 유전자 가위 방법을 이용하여 *MYH8* R1292X 세포주를 구축하였다. F-actin과 vinculin의 형광염색과 상처 치유 분석, 그리고 부착 분석을 통해 세

포의 이동능을 평가하였을 때 돌연변이 세포에서 이동능이 유의하게 증가되어 있음을 확인하였고, 더 나아가 세포 이동에 용이하도록 세포 모양과 세포 주기가 변화되어 있음을 확인하였다. 높은 이동능과 종양의 악성화와 관련된 상피-간엽 이동 관련 분자인 Snail, Slug, ZEB1 역시 돌연변이 세포에서 증가되어 있었으며 분자신호 분자 스크리닝과 약물처리 실험을 통해 Raf/MAPK 신호전달 경로가 이러한 특징의 주요 조절 인자임을 밝혔다. 본 연구 결과를 종합하면, *MYH8* 절단돌연변이 R1292X 는 세포 모양의 변화, 증가된 이동성 그리고 상피-간엽 이동 특징을 유도하며 이러한 유도된 특징들이 급성골수성백혈병 진행과 나쁜 예후와 관련이 있을 수 있음을 보여준다.

주 요 어: 급성골수성백혈병, *KIT*, 핌 키나아제, *MYH8*, 절단 돌연변이, 세포생존, 세포이동, 상피-간엽 이동

학 번: 2014-22027